Elsevier Editorial System(tm) for Journal of Volcanology and Geothermal Research

Manuscript Draft

Manuscript Number: VOLGEO2875R1

Title: New geological insights and structural control on fluid circulation in La Fossa cone (Vulcano, Aeolian Islands, Italy)

Article Type: Research Paper

Keywords: Electrical resistivity; self-potential; soil CO2 degassing; temperature; fluid circulation; hydrothermal system; structural boundary; Vulcano; La Fossa cone

Corresponding Author: Dr Stéphanie Barde-Cabusson, Ph.D.

Corresponding Author's Institution: Università Degli Studi di Firenze

First Author: Stéphanie Barde-Cabusson, Ph.D.

Order of Authors: Stéphanie Barde-Cabusson, Ph.D.; Anthony Finizola; André Revil; Tullio Ricci; Sabatino Piscitelli; Enzo Rizzo; Bernard Angeletti; Marianna Balasco; Laura Bennati; Svetlana Byrdina; Nicolo Carzaniga; Agnès Crespy; Fabio Di Gangi; Julie Morin; Angela Perrone; Matteo Rossi; Emilie Roulleau; Barbara Suski; Nicolas Villeneuve

Abstract: Electric resistivity tomography (ERT), self-potential (SP), soil CO2 flux, and temperature are used to study the inner structure of La Fossa cone (Vulcano, Aeolian Islands). Nine profiles were performed across the cone with a measurement spacing of 20 m. The crater rims of La Fossa cone are underlined by sharp horizontal resistivity contrasts. SP, CO2 flux, and temperature anomalies underline these boundaries which we interpret as structural limits associated to preferential circulation of fluids. The Pietre Cotte crater and Gran Cratere craters enclose the main hydrothermal system, identified at the centre of the edifice on the base of low electrical resistivity values (< 20 Ω.m) and strong CO2 degassing, SP, and temperature anomalies. In the periphery, the hydrothermal activity is also visible along structural boundaries such as the Punte Nere, Forgia

Vecchia, and Palizzi crater rims and at the base of the cone, on the southern side of the edifice, along a fault attributed to the NW main tectonic trend of the island. Inside the Punte Nere crater, the ERT sections show an electrical resistive body that we interpret as an intrusion or a dome. This magmatic body is reconstructed in 3D using the available ERT profiles. Its shape and position, with respect to the Pietre Cotte crater fault, allows replacing this structure in the chronology of the development of the volcano. It corresponds to a late phase of activity of the Punte Nere edifice. Considering the position of the SP, soil CO2 flux, and temperature maxima and the repartition of conductive zones related to hydrothermal circulation with respect to the main structural features, La Fossa cone could be considered as a relevant example of the strong influence of pre-existing structures on hydrothermal fluid circulation at the scale of a volcanic edifice.

Stéphanie Barde-Cabusson
Dipartimento di Scienze della Terra,
Università Degli Studi di Firenze, Italy
Email : s.barde.cabusson@gmail.com
Tel. +39-055-2757479 ; Fax +39-055-2756242)

Italy, May 27th, 2009

Dear Dr. Joan Marti,

Please find attached the revised version of our manuscript entitled "New geological insights and structural control on fluid circulation in La Fossa cone (Vulcano, Aeolian Islands, Italy)" intended for publication in Journal of Volcanology and Geothermal Research.

This paper presenting new insights into the geology and the fluid circulation pattern on Vulcano (Aeolian Islands, Italy) have been revised incorporating major modifications following your comments and the two referees' remarks.

The resubmission contains the following files:

A "revision notes" file where we explain how and where each point of the reviewers' comments has been incorporated ("Barde-et-al_RevisionNotes.doc").

An annotated version of the revised manuscript where all the modifications from the initial version have been highlighted ("Barde-et-al_manuscript_revised-marked.doc").

A revised (but not annotated) version of the manuscript where all the modifications have been integrated and are not highlighted ("Barde-et-al_manuscript_revised.doc").

The 10 figures among which figure 1 and 3 have been modified since the initial submission.

The order of the authors has been slightly modified. This will be precise during the resubmission.

We carefully checked that the manuscript follows the format and layout required by JVGR. The references in the text and the references list have been verified and updated with the new version.

Kind regards,

Stéphanie Barde-Cabusson (corresponding author)

*** Revision Notes**
Click here to download Revision Notes: Barde-et-al_RevisionNotes.doc

Revision notes

-

New geological insights and structural control on fluid circulation in La Fossa cone (Vulcano, Aeolian Islands, Italy)

IMPORTANT NOTES:
* The minor corrections proposed by the reviewers and accepted by the authors are not listed inhere. However they are highlighted in yellow, as all the modifications performed on the initial manuscript, in the file "Barde-et-al_manuscript_revised-marked.doc".
* In the present file, the remarks from the reviewers are highlighted by green colour for more clarity.
* The titles and lines herein refer to the file "Barde-et-al_manuscript_revised-marked.doc".
* The list below shows the modifications requiring more explanations and the modifications not accepted.

REVIEWER 1 AND 2 MAJOR COMMENT:

A major comment of Reviewer 1 and 2 was the absence of CO_2 and SP maps. These maps were not inserted in the first version of the manuscript because it does not provide additional information with regard to the temperature map. Another reason was that these maps present distortions probably due to the variations the volcanic activity and probably of environmental parameters between the surveys. The temperature data seems less affected by these variations so that we presented it in the original manuscript.

However, we added the SP and CO2 maps in the new version and discussed their reliability in a new sub-section entitled: **4.1. Reliability of the temperature, CO_2, and SP maps**.

The other sub-sections of this section have been slightly developed with the description of the additional maps, in correlation with the temperature map.

REVIEWER 1 (JEAN-FRANÇOIS LENAT):

Abstract:
Only minor revisions, evidenced in the file "Barde-et-al_manuscript_revised-marked.doc"

1. Introduction
Only minor revisions, evidenced in the file "Barde-et-al_manuscript_revised-marked.doc"

2. Geological settings:

Line 137 - "unconformable with respect to the arc layout" was not replaced by "oblique to the arc layout" because they seem both meaningful.

Line 138 – ***Modification proposed by the reviewer:*** "This volcanic lineament ~~characteristic~~ is explained by the presence of ~~a~~ the ~~magmatic activity controlled by~~ regional ~~tectonics. Indeed, the development of these islands is strongly influenced by an active crustal discontinuity related to the~~ Tindari-Letojanni dextral strike-slip fault system formed in the continuation of the Malta escarpment (Barberi et al., 1994; Ventura, 1994; Ghisetti, 1979).

The modification proposed by the reviewer is less detailed than the initial text, we prefer keeping a slightly longer text for describing the tectonic context. Only "characteristic" was replaced by "volcanic lineament".

Comment of the reviewer: "It could be useful to signal that drill holes have shown the presence of elevated temperatures at depth and have provided information on the structure and rocks."

Considering that the location of the drill holes (Isola di Vulcano I, Isola di Vulcano Id, Vulcano Porto 1, Vulcano IIbis) is peripherical with respect to our study area we did not consider this aspect.

3. Data acquisition and processing:

This section has been renamed and organized in sections related to every method used during the survey, as suggested by the reviewer.

Line 201-208 – The introductive paragraph of this section has been corrected following most of the propositions of the reviewer (only minor corrections).

Line 206 – In the original version we precised that "The different methods used during the surveys are described in detail in Revil et al. (2008). We just summarize the main points here". We think that this replies to the comment of the reviewer:

"The thing that troubles me here is that the data acquisition has already been described (and in more details) in the paper by Revil et al. Perhaps the authors should just try to summarize those aspects (this is more or less what they do) and make a clear reference to the other paper where the reader could find the details."

Line 219 – Revil et al. (2008) detailed the inversion process and discussed the RMS errors and the tests run on the data concluding to the reliability of the dataset and of the inversion models. We added a clear reference to this work in the text.

Add proposed by the reviewer: "Could you have made a 3D inversion ?"

A 3D modelling of the data is currently in process, based on other inversion processing methods but it will be the object of a further work requiring an individual manuscript.

Line 255 – Type A correspond to a specification of the spectrometer model (volume of the accumulation chamber).

Line 274 to 278 - This last paragraph was moved here and modified from the next section (the former-manuscript section *4.1. Temperature map*).

4. Results

Replying to a major revision proposed by reviewer 1, this section has been divided in more sub-sections and the titles of the sub-sections have been modified in order to clarify the organisation of the text. These sub-sections now refer to the various areas studied and the different geological features highlighted by this study.

4.2. The central hydrothermal system

Line 324 – Minor correction not made: "The most striking information ~~provided by the global temperature map~~ is that…". The text before this sentence has been modified and we must precise here that we are talking about the global temperature map.

Line 329 – Remark from the reviewer: "Do you mean that you present a map based only on measurements taken outside the very high temperature fumaroles". Yes, as specified in the text, no measurement was made right on the fumaroles in order to prevent damages on the measurement devices.

Figures:

Figure 1:

- One of the inserts was replaced by a sketch of the tectonic context.
- The intern caption was modified from "Recent sediments and inhabited areas" to "Recent sediments" as the area covered by the sediments is larger and surrounds the area covered by the inhabited area.
- The location "Palizzi" has been added.

Figure captions:

Figure 1: the caption has been modified to describe the insert of the tectonic context added to the figure.

Figure 3: the caption has been modified to describe the insertion of the SP and CO_2 maps.

Additional remarks from reviewer 1:

-"One last thing. Although I am not an expert in tectonics, I was very surprised by the dips of some faults on figure 9. They suggest thrust (reverse) faulting. Maybe the authors could check this."

The inversion model (figure 9 and 10) clearly highlights an outward dip of the south-western border fault of Gran Crater marked by the sharp resistivity transition. This dip is common in case of caldera-type or pit-crater-type collapse of a crater roof (Anderson, 1936; Branney, 1995; Acocella et al., 2000; Roche et al., 2000 and 2001; Walter and Troll, 2001). This crater could have been affected by this type of collapse during the crater formation. A similar dipping is not observed on the north-eastern border maybe because the collapse was asymmetric and/or perturbations due to hydrothermal circulations and alteration in the vicinity of the eastern resustive body evidenced (Cf. section 4.6. The eastern electrical resistive body). A paragraph has been added taking those remarks into consideration → **line 516-523**.

Reviewer 2 (Anonymous):

----

1. Introduction

Line 70 - Reference to Aubert and Baubron added in the text (also inside the References section).

2. Geological setting

Comment of the reviewer: "This chapter can be shortened if necessary"

We decided not to reduce this part due to the importance of the link between the geology and the geophysical approach in our study.

3. Data acquisition – (and general comment of the reviewer)

This section has been renamed "3. Data acquisition and processing"
In this section we only made general remarks about the possible interpretation of ERT, SP, soil CO_2 flux and temperature data. The discussions and interpretations of our data is presented in the next section "4. Results".

The reviewer ask to detail "the choice of parameters for RES2DINV inversion, the obtained RMS (for example synthetic Table of the RMS), possible variations of models,…".
We did not present these descriptions because it was detailed in Revil at al. (2008) →

Section 3.1. describes the inversion method used with RES2DINV

Section 5.1. discuss the uncertainty associated with the resistivity data related to the RMS obtained for the inversions.

Line 241 - As proposed by the reviewer, the reference Aubert and Kieffer (1984) was replaced by the reference Aubert and Lima (1986). The complete reference has also been inserted in the References section.

4. Results

Line 480-483 -
- Reviewer 2 ask "Add explanation about low resistivity of tuff deposits"

The resistivity of the terrain depends mainly on the interconnected porosity of the rock and on the resistivity of the pore fluids. On Vulcano, the tuff layers guide hydrothermal fluid circulations. The high conductivity values observed, result from the cation exchange capacity of clay minerals and zeolites composing the Vulcano tuff. It is also indicative of the alteration of the rock (see Roberts and Lin, 1997; Revil et al., 2002; Bernard et al., 2007).
We added this explanation in the text.

Comment of the reviewer: do not confuse variation and gradient; you must use in this case variations and not gradients (see also line 462 and 684 (caption Figure 6))
The term "gradient" has been replaced for all the cases highlighted by the reviewer.

5. Conclusions

Comment of the reviewer: "It is not obvious that the N-W end of profile 4 could be the best choice for monitoring the the hydrothermal variations. You probably have to take into account the influence of the sea."

Due to its distal location, the monitoring of this particular anomaly seems an interesting test area. The variations could be correlated to other monitoring stations located in the summit area to discriminate "parasitic" signal (sea, etc…).

Figure 4

Comment of the reviewer: "the transition is sharp on the West boundary but not on the East boundary GC and PC for SP and CO_2. This case, also others cases (Figures 5, 7, 8) could be developped."

The asymmetry of the temperature anomalies have been discussed in the text but concerning SP and CO_2, this point does not seem relevant.

New geological insights and structural control on fluid circulation in La Fossa cone (Vulcano, Aeolian Islands, Italy)

Barde Cabusson S. (1, 2), Finizola A. (3, 4), Revil A. (5, 6), Ricci T. (7), Piscitelli S. (8), Rizzo E. (8), Angeletti B. (9), Balasco M. (8), Bennati L. (10), Byrdina S. (2, 11), Carzaniga N. (12), Crespy A. (9), Di Gangi F. (4), Morin J. (3, 13), Perrone A. (8), Rossi M. (14, 12), Roulleau E. (15), Suski B. (16, 9), Villeneuve N. (17)

(1) Dipartimento di Scienze della Terra, Università Degli Studi di Firenze, Italy
(2) LMV, Université Blaise Pascal, Clermont-Ferrand, France
(3) Laboratoire GéoSciences Réunion, UR, IPGP, UMR 7154, Saint-Denis, La Réunion, France
(4) Istituto Nazionale di Geofisica e Vulcanologia, Palermo, Italy
(5) Colorado School of Mines, Dept. of Geophysics, Golden, CO, USA
(6) CNRS-LGIT (UMR 5559), University of Savoie, Equipe Volcan, Chambéry, France
(7) Istituto Nazionale di Geofisica e Vulcanologia, Roma, Italy
(8) IMAA-CNR, Laboratory of Geophysics Tito Scalo (PZ), Italy
(9) CNRS-CEREGE, Université Paul Cézanne, Aix en Provence, France
(10) Dept. of Earth & Atmospheric Sciences, Purdue University, West Lafayette, USA
(11) Equipe de Géomagnétisme, IPGP, UMR 7154, 4, Place Jussieu, 75005 Paris, France
(12) Università Milano-Bicocca, Milan, Italy
(13) Université Paris 1, Panthéon-Sorbonne, Paris, France
(14) Dipartimento di Geoscienze, Università di Padova, Italy
(15) GEOTOP-UQAM-McGill, Montréal, Canada
(16) Université de Lausanne (UNIL), Institut de Géophysique, Lausanne, Switzerland
(17) Institut de Recherche pour le Développement, US 140 ESPACE, La Réunion, France

---

Corresponding author :
Stéphanie Barde-Cabusson (Dipartimento di Scienze della Terra, Università di Firenze, Via Giorgio La Pira 4, 50121, Firenze, Italy; email : s.barde.cabusson@gmail.com; Tel. +39-055-2757479 ; Fax +39-055-2756242)

Abstract

Electric resistivity tomography (ERT), self-potential (SP), soil CO_2 flux, and temperature are used to study the inner structure of La Fossa cone (Vulcano, Aeolian Islands). Nine profiles were performed across the cone with a measurement spacing of 20 m. The crater rims of La Fossa cone are underlined by sharp horizontal resistivity contrasts. SP, CO_2 flux, and temperature anomalies underline these boundaries which we interpret as structural limits associated to preferential circulation of fluids. The Pietre Cotte crater and Gran Cratere craters enclose the main hydrothermal system, identified at the centre of the edifice on the base of low electrical resistivity values (< 20 Ω.m) and strong CO_2 degassing, SP, and temperature anomalies. In the periphery, the hydrothermal activity is also visible along structural boundaries such as the Punte Nere, Forgia Vecchia, and Palizzi crater rims and at the base of the cone, on the southern side of the edifice, along a fault attributed to the NW main tectonic trend of the island. Inside the Punte Nere crater, the ERT sections show an electrical resistive body that we interpret as an intrusion or a dome. This magmatic body is reconstructed in 3D using the available ERT profiles. Its shape and position, with respect to the Pietre Cotte crater fault, allows replacing this structure in the chronology of the development of the volcano. It corresponds to a late phase of activity of the Punte Nere edifice. Considering the position of the SP, soil CO_2 flux, and temperature maxima and the repartition of conductive zones related to hydrothermal circulation with respect to the main structural features, La Fossa cone could be considered as a relevant example of the strong influence of pre-existing structures on hydrothermal fluid circulation at the scale of a volcanic edifice.

Keywords: Electrical resistivity; self-potential; soil CO_2 degassing; temperature; fluid circulation; hydrothermal system; structural boundary; Vulcano; La Fossa cone.

Short title: Structural control on fluid circulation

1. Introduction

Active volcanoes are not only the place of magma transfers but also of permanent heat and fluid transfers from the magma reservoir to the surface, even during long periods of eruptive quiescence. These exchanges are mainly insured by convective circulations of hot ground fluids (gas and liquids) inside the hydrothermal system (e.g., Aubert and Baubron, 1988; Granieri et al., 2006; Finizola et al., 2003, 2006).

A volcanic edifice can be a very heterogeneous structure due to its eruptive dynamics and evolution. It is usually shaped by an alternation of lava flow units, ash layers, volcanoclastic deposits, clay-rich materials resulting from hydrothermal alteration, various intrusions, all heterogeneously affected by deformation and the presence of cracks. During its evolution, more permeable levels and interfaces develop owing to the superposition of the various geological units. However, structural limits and fracture zones formed inside the volcano along its history can constitute the more permeable zones. These weakness planes allow the infiltration of meteoric waters, the rise of hydrothermal fluids, and sometimes the transfer of magma. A good example is provided by caldera structures, where the hydrothermal activity concentrates along the border fault and on intracalderic fractures (e.g., Pribnow et al., 2003). In a comparative study of the Valles caldera (New Mexico) and of the calderas of Lake City and Platoro (Colorado), Wohletz and Heiken (1992) highlights that the hydrothermal alteration develops principally along the faults formed inside the caldera and around shallow intrusions. Also, the craters boundaries being highly permeable zones of the edifice, they usually guide fluid circulation in the same way (e.g., Revil et al., 2004). In addition to these localized pathways, the transfers can be more pervasive depending on the permeability of the volcanic materials, e.g., the diffuse degassing of CO_2 (Baubron et al., 1990; Allard et al., 1991).

The hydrothermal activity can also alter the cohesion of rocks and therefore be responsible for large collapses and landslides or for the spreading of volcanic edifices (Lopez and Williams, 1993; Day, 1996; Vallance and Scott, 1997; Voight and Elsworth, 1997; van Wyk de Vries et al., 2000; Reid et al., 2001; Cecchi et al., 2005; Merle and Lénat, 2003). The hydrothermal alteration, in addition to increasing the risk of instability, also enhances the mobility of the debris avalanches. Indeed, the hydrothermal alteration reduces the cohesion of the rock and increases the fluid content favouring these risks (e.g., Vallance and Scott 1997). On Vulcano, a landslide occurred the 20th April 1988 on the north-eastern flank of La Fossa cone. A volume of 220.000 m^3 of superficial pyroclastic deposits was implicated. This destabilization was contemporary of the opening of fractures affected by fumarolic emanations and hydrothermal alteration (Ricci, 2007). Currently, given the strong alteration of the rocks around the Forgia Vecchia (north-north-east flank) this area is of major landslide-probability and, due to the population density, in particular during the tourist season, it presents a major risk. Understanding the relationships between pre-existing structures and fluid circulation is important to study volcanic hydrothermal systems and could help to forecast possible volcanic instabilities in the long term.

Because drilling volcanic edifices is difficult, non-intrusive methods that can image the structure of a volcanic edifice and that can be sensitive to the flow of the ground water and CO_2 are important to understand the dynamics of hydrothermal systems. They constitute very important tools to extrapolate the observations made at the ground surface to depth in order to draw a map of the geohazards associated with a volcanic edifice. La Fossa cone (Vulcano, Aeolian Islands, Italy) is a small and complex volcanic edifice characterized by a strong alteration due to a very active hydrothermal system. In addition, we have a good knowledge regarding its eruptive history (De Astis et al., 2007 and references therein). It is therefore an ideal natural laboratory to conduct a high resolution survey investigating the structure and the hydrothermal system of a volcanic edifice.

We acquired multi-electrode electric resistivity data (ERT), self potential (SP), soil CO_2 diffuse degassing, and shallow ground temperature data along several profiles. The same dataset was used by Revil et al. (2008) to present the main structural features interpreted from some of the profiles and to perform a numerical modelling of the ground water flow pattern. In our case, this multidisciplinary study is used to map the signature of the hydrothermal activity of La Fossa cone and to detail its inner structure above the sea level.

The main goals of this study are (1) to interpret the data in terms of geological features and (2) to understand how pre-existing geological structures control the pattern of fluid circulation.

2. Geological setting

Located in the south of Tyrrhenian Basin, Vulcano is the third largest of the seven Aeolian Islands. It is also the southernmost island of the archipelago. Salina, Lipari, and Vulcano are three islands aligned along a NNW-SSE trend, unconformable with respect to the arc layout. This volcanic lineament is explained by a magmatic activity controlled by regional tectonics. Indeed, the development of these islands is strongly influenced by an active crustal discontinuity related to the Tindari-Letojanni dextral strike-slip fault system formed in the continuation of the Malta escarpment (Barberi et al., 1994; Ventura, 1994; Ghisetti, 1979). The horizontal displacements along the strike-slip system are accommodated by N-S to NE-SW trending normal faults and accompanied by pure extension (Mazzuoli et al., 1995).

Vulcano Island was built by a succession of constructive and destructive stages of the two main edifices, Vulcano Primordiale and La Fossa cone (Fig. 1). Vulcano Primordiale is the oldest (120-100 ka, see Keller, 1980). This unit, located in the southern part on the island, is also commonly named Piano or Serro di Punta Lunga. This stratovolcano has been truncated around 100 ka by the collapse of the Piano Caldera, now filled by post-collapse eruptive materials (De Astis et al., 1989). The eruptive centre has then migrated to the north-west to form the Cardo tuff cone and the Lentia intrusive Complex. Both have been largely masked owing to the collapse of La Fossa Caldera and because of the edification of La Fossa cone inside the caldera depression (De Astis et al., 2007).

La Fossa cone is a 391 m height stratocone, active since ~6000 years (Dellino and La Volpe, 1997; De Rosa et al., 2004). Its eruptive history and structure have been studied by many authors (e.g., Keller, 1970, 1980; Frazzetta et al., 1983, 1984; Dellino and La Volpe 1997; De Astis et al., 1997, 2003, Arrighi et al., 2006). The present day edifice results from six main phases of activity described in the last issue of the geological map of the island (De Astis et al., 2007) which we simplified in Figure 1.

(1) Punte Nere formation is composed of pyroclastic products corresponding to surges and fallouts deposits at the base. The upper unit is a succession of aa lava flows. This formation constitutes the former Fossa cone, associated to Punte Nere crater (PN) and now truncated to the west by the younger cone.

(2) Palizzi formation is composed of three units. The first unit show a pyroclastic succession of varicoloured ashes ("Tufi varicolori di La Fossa"). Two younger units display an alternation of pyroclastic deposits and lava flows. In the meantime, a new eruptive centre was active in the northern part of the island, forming the Vulcanello peninsula. The corresponding crater rim (Pa) is nowadays only visible on the southern part of La Fossa cone.

(3) Caruggi formation, previously named Commenda (Frazzetta et al., 1984; Arrighi et al., 2006) consists of pyroclastic deposits with yellow-reddish ashes and rounded, hydrothermalized lithic blocks. The upper unit corresponds to varicoloured tuffs and ash layers. This layer is well recognized in the landscape as pink coloured outcrops.

(4) Forgia Vecchia formation has settled on the northern flank of La Fossa cone and is made up of lahar deposits. This stage also left an adventive crater (FV), approximately 300 m wide, on the northern flank.
(5) Pietre Cotte formation consists of a pyroclastic unit mainly visible on the southern flank of La Fossa cone. The cycle is ended by the emission of a striking tongue-like rhyolitic lava flow easily recognisable on the northwest flank. The corresponding crater of Pietre Cotte stage (PC) intersects both PN and Pa craters.
(6) Gran Cratere formation is a pyroclastic level clearly visible on the major part of La Fossa cone as grey ashes. This stage of activity ended with the historical 1888-1890 eruption and gave rise to the formation of a succession of nested craters (GC) partly overlapping the PC crater rim.

The current activity on Vulcano is characterized by intense fumarolic emissions in La Fossa crater, on the northern and southern flanks of the edifice and in the area of the Porto di Levante harbour. Other isolated fumaroles have been observed on the flanks of the edifice while a strong cold degassing is localized in the Palizzi area. Since 1890 the quiescent La Fossa volcano is characterized by the occurrence of "crises" (Granieri et al., 2006) with strong increases of the fumaroles temperatures and output and variations of the chemical compositions toward more magmatic signatures caused by the uprising of magmatic gas. Moreover, a local anomalous shallow seismicity characterized by swarms of low-magnitude, due to rising gases in the fumarolic feeding system, an increase of the diffuse soil CO_2 degassing, and a spatial expansion of the fumarolic fields are also characteristic of these "crises" but no evidence of magma uprising was signaled.

3. Data acquisition and processing

In October 2005, May 2006 and October 2006 we performed three multidisciplinary surveys. Nine profiles were deployed crossing the entire edifice, for a total length of 18980 m (Fig. 2). We acquired multi-electrode electrical resistivity data with an electrode spacing of 20 m. Self potential, CO_2, and temperature measurements were acquired on the same points, which represent 957 measurements for these methods. The methods used during the surveys are described in detail in Revil et al. (2008). We summarize the main points here:

3.1. Electric resistivity tomography

Resistivity measurements were acquired with an ABEM (SAS4000) resistivimeter with a multichannel system of 64 electrodes connected to the acquisition system through a 1260 m long cable. We used a Wenner array because of its good signal-to-noise ratio. We added salty water around each electrode to decrease the contact resistance between the electrodes and the ground. Two or three roll-along were performed to complete each profile. The apparent resistivity values obtained were inverted by RES2DINV software (Geotomo software; Griffiths and Barker, 1993; Loke and Barker, 1996) obtaining a resistivity model along each section. Revil et al. (2008) detailed the inversion process and discussed the results of the tests run to check the uncertainty associated with the resistivity data. The authors conclude that the inverse modelling used is very robust to the noise existing in the raw data. The results allow visualizing a model of resistivity of the edifice. Some of the most representative resistivity models will be presented below as 2D cross-sections.

The interpretation of inverted data alone is a notoriously difficult task because electrical resistivity varies with a number of parameters including temperature, salinity, clay and zeolite contents and mineralogy, grain shape, and porosity (Revil et al., 2002; Rabaute et al., 2003). For the same data set, there are several possible resistivity models that fit the data equally well (e.g., Auken and Christiansen, 2004; Binley and Kemna, 2005). However, the resistivity models highlight clear spatial resistivity contrasts that can be interpreted in terms of lithology transitions.

3.2. Self potential

SP measurements were performed using a pair of non-polarizing $Cu/CuSO_4$ electrodes. The difference of electrical potential between the reference electrode (conventionally placed at the beginning of the profile) and the scanning electrode was measured with a calibrated high impedance voltmeter with a sensitivity of 0.1 mV. The SP method allows to map rising hydrothermal fluids on active volcanoes; e.g., on Kilauea in Hawaii (Zablocki, 1976), on Nevado de Colima and Fuego de Colima in Mexico (Aubert and Lima, 1986), on Piton de la Fournaise in Reunion Island (Malengreau et al., 1994 and Michel and Zlotnicki, 1998), on the Karthala in Comoros (Durand, 1997; Lénat et al., 1998), on Stromboli in Italy (Finizola et al., 2002), and on Misti volcano in Peru (Finizola et al., 2004). In the present case, this method was useful to highlight the structural limits, which are usually preferential paths for ground water circulation and to map the hydrothermal activity.

3.3. Soil CO_2 flux

Soil CO_2 flux measurements were acquired using the methodology described by Chiodini et al. (1998). The instrumentation consists of an IR spectrometer Licor LI800 with a range of 0 to 2000 μmol/mol (2 % vol.), an accumulation chamber (type A: volume of 30 cm^3) and a palmtop to plot the CO_2 increase as a function of time. The accumulation chamber is leaned on the ground so that the atmospheric air cannot penetrate inside. The gas permeating from the soil accumulates in the dead volume, passes through the IR spectrometer and is re-injected in the accumulation chamber. The increase of the concentration in the chamber through time allows determining the flux of CO_2 from the soil. This is a powerful method to detect preferential hydrothermal flux paths on a volcanic edifice.

3.4. Temperature at 30 cm depth

Temperature measurements were performed at a depth of 30 cm ± 1 cm and respecting a stabilisation time of 15 minutes. We used thermal probes and a digital thermometer with a sensitivity of 0.1°C. The maximum amplitude of diurnal variation at Vulcano at 30 cm depth during the summer season is less than 1.2°C (Chébli, 1997; Aubert et al., 2007). During the year, at that depth, the temperature varies from 12.2 to 27.2°C in January and August, respectively (Lo Cascio and Navarra, 1997). Consequently, for measurements performed at 30 cm depth, we consider a temperature above 30°C as a signature of hydrothermal fluid circulations.

We made a temperature map interpolated from the data of the nine profiles (Fig. 3a). The data have been acquired within one year so that the amplitude of the thermal anomalies probably varied along the period of acquisition of the dataset due to seasonal and internal variations. However this figure gives reliable qualitative information.

4. Results

4.1. Reliability of the temperature, CO_2, and SP maps

A map is supposed to present the state of a particular area within a short period of time, which suggests that the conditions along the acquisition of a dataset must remain relatively stable. Our dataset contains data from three surveys performed in a one year period (from October 2005 to October 2006). Concerning the SP measurements, we added a few data from a survey of 2004 (black dots on Figure 3b) in order to join the profiles to the sea, calculate a closure offset and distribute linearly this offset on the profiles to correct the global dataset presented here. Knowing that, we must take into account that some parameters influencing the measurements have undergone some variations, which can distort the maps. These parameters are the volcanic activity, the soil characteristics and the atmospheric conditions.

It seems that the temperature measurements at 30 cm depth are less affected by the variations undergone between our three surveys. It is true since the measurements are not performed during rain events. In fact the rain makes the temperature fall down of several degrees depending on the depth of infiltration of the meteoric water and the atmospheric temperature.

For the SP map, some strong positive and negative anomalies remain uncorrelated with the other methods and the main information is displayed in the PC/GC crater area and the PN crater. Variations of the volcanic activity, seasonal variations of the soil moisture are the possible responsible of some of the unexplained anomalies. The contrasts of resistivity of the terrain can also affect the SP measurements without affecting the CO_2 and temperature values.

The values of the soil diffuse degassing at La Fossa volcano during the last crisis, begun at the end of 2004, revealed fluctuations of CO_2 flux until one order of magnitude (Granieri et al., 2006). It was characterized by significant variations in the extension of the anomalous degassing area. The CO_2 flux data presented in this paper were collected in three different periods during the last crisis of La Fossa volcano. Consequently, the resulting CO_2 map of the entire La Fossa cone shown in Figure 3c is purely indicative because of the fluctuations in the degassing activity and no quantitative analyses can be done. Nevertheless the CO_2 map closely reflects the shape of the anomalous degassing areas presented by Granieri et al. (2006).

Finally, more than giving quantitative information, the temperature, SP, and CO_2 maps are useful to get qualitative information, i.e. structural information and a distribution of the hydrothermal emissions. Based on the correlations between these maps, several areas of interest have been identified and will be commented below.

4.2. The central hydrothermal system

In an interpolated map, the less the profiles are spaced, the more the interpolation is reliable so that, on the temperature, SP, and CO_2 maps, the most relevant information is concentrated around the data points (white and black dots on Figure 3). The most striking information provided by the global temperature map (Figure 3a) is that the main thermal anomaly is bounded by the rim of the GC and PC craters, which are the most recent craters formed on La Fossa cone. This central thermal anomaly is correlated to anomalies of similar extension in SP and soil CO_2 flux (maps in Figure 3b and 3c).

The highest temperatures have been measured into the inner crater. Gases escape from the fumaroles at high temperature (~400°C) and, for the safety of the measuring devices, no measurement was made right on it. In the north-east area, the thermal, SP and CO_2 anomalies extend beyond the GC rim, between the GC and the PC crater rims. In the field, these zones correspond to strong fumarolic activity and/or extensive hydrothermal alteration. The main fumarolic field is indeed located on the northern wall of the GC crater, on the rim, and extends beyond its limits (see Bukumirovic et al., 1997). On Vulcano, the temperatures of the fumaroles can reach several hundred degrees Celsius (almost 700°C during the 1977 crisis, see Barberi et al., 1991). Except on these particular locations, no measurement of our surveys overtakes 98°C. This can be explained by the presence, at depth, of a hot aquifer or of a shallow condensation zone formed under a sealed layer, acting as a thermal buffer between the magmatic heat source and the surface (Montalto 1994; Aubert et al., 2007).

These main thermal, SP, and CO_2 anomalies are the expression of the central active hydrothermal system activity and the data show that this hydrothermal system is bounded by the PC and GC crater faults.

4.3. Hydrothermal circulations along former structural limits

Hydrothermal fluid circulation is not restricted to the central crater area. Outside of the main Fossa craters area, we also identified few temperature, SP, and CO_2 anomalies. Not far from the central hydrothermal system, strong anomalies have been observed beyond the PC crater rim, on the northwest upper flank of the cone, right on the former footpath to the summit (see the central part of profile 2 in Figure 3). These high temperatures, SP, and CO_2 values are associated with fumarolic emissions.

4.3.1 Forgia Vecchia crater

On the northern flank, the Forgia Vecchia crater (FV) is affected by a thermal anomaly on its northern border (see northern section of Profile 3 on Figure 3a). The temperature measured is ~10°C above the mean temperature in this area. This is the only sign of current activity on this adventive crater, in our dataset. The FV crater border is a permeable limit acting as a guide for fluid circulation. The thermal release noticed here can be due to the presence, at shallow depth, of a still cooling magmatic batch related to the past activity. Another source could be distal hot fluid circulations associated to the current hydrothermal system of La Fossa cone.

4.3.2 Palizzi crater

On the southern flank of the edifice, Profiles 3, 5, and 6 display thermal and CO_2 anomalies on their intersection with the Pa crater rim. This crater rim is clearly underlined, even when the topography gives no evidence for it. The location of the anomalies coincides with the crater drawn by De Astis et al. (2007) in their geological map of Vulcano.

4.3.3 Punte Nere crater

One striking result is the observation of high temperature, SP, and CO_2 values in the area enclosed by the Punte Nere crater (PN), where no eruptive activity took place since 3.8 ka (De Astis et al., 2007). As shown by the data along the two profiles crossing the rim in the North (Profile 6) and in the East (Profile 8), the thermal and CO_2 anomalies extend outside the PN crater, on the upper part of the slope of the cone.

Two types of thermal anomalies can be distinguished in this area, which are (1) strong anomalies (in the range between 35°C and 60°C) along structural limits and (2) weak anomalies (smaller than 35°C) in areas poorly or unaffected by faulting. On Profiles 6 and 8, the temperature anomalies show that hydrothermal fluids take advantage of the high permeability along the crater rim to reach the ground surface. The maximum temperature registered is ~60°C. In this case, the heat can come from a deep source and produce strong anomalies in the vicinity of the ground surface. Concerning the wide anomalous temperature field inside the PN crater, temperatures reach a maximum of 35°C.

As for the FV crater but to a wider scale, the PN crater anomaly can have two potential origins: the hot-fluid source can be due either to circulations of fluids from La Fossa hydrothermal system or to remnants of the past activity of the Punte Nere cone. Profile 1 can help determining the source (Fig. 4). As on the maps (Fig. 3), an overview of this profile shows high values of temperature, self-potential, and CO_2 in the central part of the edifice. The self-potential data display a typical W shape (e.g., Ishido, 2004), confirming that the main hydrothermal activity is concentrated in the limits of the GC crater. Crossing the eastern side of the GC crater rim, the temperature and CO_2 progressively decrease from west to east, inside the PN crater. The anomaly vanishes to reach characteristic temperatures of "cold" zones on the flank of the edifice. At depth, the resistivity structure shows a continuous conductive zone from the most internal crater to the flank of the cone. In the limits of the PC crater, the low resistivity is associated to the hydrothermal system, i.e. hydrothermal fluids convecting through the detritic volcanic deposits of the last phases of eruptive activity. Beyond the PC crater, we interpret the low resistivity layer as tuff deposits from La Fossa activity. The resistive body visible at depth acts as an impermeable limit so that the fluids are guided inside the more permeable overlying tuff level. Underground, the hot fluids rising from the central zone overflow to the east into the PN crater and progressively loose gases and heat. The temperature, SP, and CO_2 anomalies visible inside the PN crater can be attributed to this phenomenon, even if a contribution of a residual degassing activity of the PN volcanic centre cannot be ruled out.

4.4. Regional faulting evidences in the Palizzi area

Profile 4 was performed at the base of the cone, from Porto di Levante to an area situated to the East of Palizzi, near the Rio Grande bed. The CO_2 map (Fig. 3c) shows remarkable anomalies in the Palizzi area. The global temperature map (Fig. 3a) does not display a perceptible anomaly along Profile 4. However, a closer inspection of the data indicates a variation of ~6°C from one extremity of the profile to the other (see Figures 5 and 6). At the south-eastern end of the profile, the temperature is ~18°C. Following the profile to Porto di Levante, the temperature increases progressively and reaches a maximum of ~24°C. The data were acquired in only two days and with similar dry meteorological conditions all along this period of time. Moreover, this progressive temperature increase of ~6°C from the southern flank to the north-western flank of La Fossa cone exceeds the maximum amplitude of diurnal variation which is less than 1.2°C at Vulcano, for measurements performed at 30 cm depth during summer season (Chébli, 1997; Aubert et al., 2007). This makes of these 6°C a significant variation.

In the northern and southern parts of the profile, the ERT model shows a shallow resistive layer associated to pyroclastic deposits. These deposits are from the Gran Cratere phase of activity in the northern portion of the profile and from the Palizzi phase in the south. This resistive layer of a few meters-thick overlays a low-resistivity medium (< 20 Ω.m). At the center of the profile, we notice the presence of a high resistivity zone. The thickness of this body globally increases from north to south. This structure is bounded by two vertical limits evidenced by sharp transitions of the resistivity. The northern boundary is rapidly blurring at depth. The southern boundary is marked by a sharpest transition of resistivity and runs from the shallow levels of the section, until the maximum depth of investigation.

On the northern part of the profile, the soil CO_2 flux decreases from north to south consistently with the global decrease of temperature observed along the whole profile. In the vicinity of the resistive body, the CO_2 flux increases, reaching a maximum in the area surrounding the southern vertical limit identified from the resistivity data. On the area surrounding the resistive body the short wave-length variations of the temperature are significantly lower than on the rest of the profile. Thereby, along our profile, the southern vertical limit of the resistive body marks a sharp increase of ~2.5°C of the mean temperature from north to south. Right on the northern boundary of the body, we also observe a slight soil CO_2 flux anomaly (~80 g/m².d) and a decrease of the SP signal (~50 mV).

Capasso et al. (2000) analysed partial pressures of He and CO_2 of some water samples from the north-eastern quarter of La Fossa cone area. They observed that the values of these partial pressures were appreciably higher than those in waters in equilibrium with the atmosphere, therefore showing interaction between volcanic gases and groundwater. Our data are consistent with those results and we interpret the gradient observed along Profile 4 as the evidence of preferential hot fluid circulations at the base of the north-western flank of La Fossa cone. The peaks of CO_2 flux in our data, around Palizzi are consistent with soil gas samples analysed by Capasso et al. (1997) in the same zone. The authors measured widespread exhalative manifestations dominated by CO_2 on Palizzi that they interpreted in terms of hydrothermal circulation. The local anomalies we observed and the associated vertical limit pointed out by the ERT data lead us to interpret this signal as hydrothermal fluid circulation rising along a volcano-tectonic structure. This structure could be related to the NNW Tindari-Letojanni regional fault system, identified in the southern sector of La Fossa caldera (Barberi et al., 1994). The northern boundary of the resistive body is not deeply rooted as is the southern one. This limit is likely only a lithological transition. The resistive rocks, probably a lava flow pile or a lava dome, constitute an impermeable limit to fluid circulation.

The anomalies registered here are likely due to circulation of fluids guided along the lithological boundary.

4.5. Comparison between the data and the geology

4.5.1. Signals associated to the various volcanic formations

The ERT data allow visualizing almost the entire cone above sea level. The profiles detailed in the following paragraphs cross the main structures identified on the volcanic edifice. In the first layers of the sections, the ERT data can be easily correlated to field observations. Indeed, in all the profiles, the Gran Cratere grey ash formation appears as a high-resistivity layer (see Figures 4, 5, 7, 8). At the base of this resistive layer, the sharp transition in electrical resistivity can be interpreted as a sharp lithological transition. Thereby this interface can be followed at depth, along the slopes of the cone. The ERT sections display a thickness of ~20-30 m which could be attributed to the presence of the Gran Cratere, the Pietre Cotte and, the Forgia Vecchia formations.

The tuff outcrops, mostly corresponding to the Palizzi and Caruggi pyroclastic formations, are correlated to low resistivity values ($< 20\ \Omega.m$). This is visible in various outcrops as in the northern part of profile 6 (Fig. 7). These low resistivity values result from the cation exchange capacity of clay minerals and zeolites composing the Vulcano tuff and are indicative of the alteration of the rock (see Roberts and Lin, 1997; Revil et al., 2002; Bernard et al., 2007).

Also in the southern part of Profile 8, the GC crater cliff shows the succession of an upper electrical resistive layer overlying a conductive layer (Fig. 8). In the field they are related respectively to (1) the Gran Cratere ash and Pietre Cotte deposits and (2) to the Caruggi tuff deposits (see the simplified geologic map of Figure 1).

4.5.2. Signals associated to the fumaroles

In the field, the fumaroles are concentrated along the most recent crater rims. The fumarolic fields inside the GC crater coincide with very low resistivity values, in the same order of magnitude than the tuffs deposits. The difference between “cold” tuffs and rocks affected by hydrothermal convection is highlighted by field observations, self-potential, temperature, and CO_2 flux measurements. Profile 6 shows highly conductive terrains

(< 20 Ω.m) right under the most active fumaroles of La Fossa cone (Fig. 7). These conductive values are correlated with a temperature anomaly reaching 95°C, a positive self-potential anomaly of 100 mV (variation with respect to the mean SP value in this zone) and a CO_2 flux peak reaching ~10,000 g/m².d in the vicinity of the fumaroles. The most striking feature is the resistivity model showing a conductive channel running from the fumaroles at the surface, to the central hydrothermal system, until the maximum depth of investigation. The channel is progressively widening with depth. It developed thanks to a pre-existent structural limit, which is the GC crater.

4.5.3. Signals associated to crater boundaries

The craters identified through the morphology of the edifice and from a previous work (De Astis et al., 2007) are correlated with sharp horizontal transitions of resistivity forming more or less vertical limits. The best example is given by the south-west border of the GC crater which is crossed by profiles 1 and 8 (figures 4 and 8). It displays a vertical to slightly reverse-slope border delimiting high resistivities (> 150 Ω.m) outside the crater and low resistivities (< 20 Ω.m) inside the crater. As seen before, at the surface, a clear anomaly in temperature, self-potential, and CO_2 flux, spots this boundary, at the base of the crater cliff. This type of configuration, related to a structural limit, can be observed for most of the crater rims identified.

The reverse dip of the crater border faults is a common consequence of caldera-type or pit-crater-type collapse of a crater roof (e.g. Anderson, 1936; Branney, 1995; Acocella et al., 2000; Roche et al., 2000 and 2001; Walter and Troll, 2001). Therefore, GC crater could have been affected by this type of collapse during its formation. A similar dipping is not observed on the north-eastern border maybe because the collapse was asymmetric. Hydrothermal circulations and alteration in the vicinity of the eastern magma body evidenced under the PN crater could also have modified the resistivity distribution appearing nowadays and distort the observation on this side (Cf. next section: 4.6. The Eastern electrical resistive body).

4.6. The eastern electrical resistive body

On all the sections crossing the eastern half of the edifice, a wide resistive body has been highlighted inside the PN crater, buried under younger formations. Profiles 1, 5, 6, 7, 8, and 9 (see Figure 2 for position of the profiles) clearly show a zone of resistivities ranging from 200 Ω.m to 1000 Ω.m, at depth. These high resistivity zones are in the range of the values expected for a lava flow pile or intrusive rocks (a dyke system, a shallow magma batch or a dome; e.g., see Figure 1.5 of Loke, 2004). The resistivity of the terrain depends mainly on the interconnected porosity of the rock and on the resistivity of the pore fluids. As an example, in a dome, a significant proportion of the vesicles are isolated and refilled by volcanic gas (e.g., see Ramsey and Fink, 1999) which confers a high resistivity to the rock.

It is important to notice that the inversion of ERT data tends to smooth the resistivity transitions i.e. the interfaces between the different geologic units. The boundary of the electrical resistive body is delimited by a sharp variation of the resistivity values, which can be associated to a lithological transition. On the resistivity models, the sharper transition is observed for an average value of ~160 Ω.m. Based on this assessment, the minimum depth of the resistive body can be estimated to ~50 m. This suggests that this unit is buried under additional formations than just the Gran Cratere pyroclastic deposits.

The density of the inverted resistivity data allowed us to reconstruct the shape of this resistive body buried inside the Punte Nere crater. To this purpose, the six ERT profiles cited above have been used. On each profile, the 160 Ω.m isoresistivity line has been digitized with one point every 20 m (in the horizontal plane). The XYZ coordinates obtained were interpolated and represented as a surface map (Fig. 9).

The lateral and vertical maximum extension of the body is not accessible as it extends under the depth of investigation. It displays a crescent shape with an irregular surface. The eastern side is a more or less regular slope, slightly steeper than the topographic surface while, to the West, the resistive body ends with a vertical boundary. This straight western limit coincides nicely with the PC crater rim.

Blanco-Montenegro et al. (2007) found a magnetic anomaly inside the PN crater. The authors interpreted this anomaly as a pile of tephritic lavas emplaced in an early phase of activity of La Fossa cone. From our ERT data, the shape, position and range of resistivity of this body led us to interpret it as an intrusion or a dome contemporary of the activity of the PN cone (5.3 ka – 3.8 ka) and truncated to the west, on at least 200 m depth by the PC crater ring fault during its formation (1739 A.D.) (See Figure 10). The presence of this large buried magma body, if it is not totally cooled down and degassed, can contribute to the thermal and CO_2 flux anomalies observed inside the PN crater (Fig. 8).

5. Conclusions

All the geophysical and geochemical anomalies we evidenced at the surface of La Fossa cone are controlled by structural limits. The main hydrothermal system is enclosed by the boundaries of the PC and GC craters. This is indicated by the low resistivity value of the formations and by the strong self-potential, CO_2 flux, and temperature anomalies measured in the limits of these craters. The hydrothermal activity is not restricted to the central part of the edifice. In the periphery, hydrothermal circulations have been evidenced and are, most of the time, clearly influenced by the structure of the edifice. This structure corresponds either to lithological levels or to structural limits and the following conclusions have been reached:

(1) The hydrothermal fluids rising from the central hydrothermal system of the GC crater condensate at shallow depth and partly flow down to the PN crater, through the more permeable levels. They are guided along the PC crater border and the resistive body highlighted at depth by electrical resistivity tomography.

(2) The Palizzi area is affected by circulations of hydrothermal fluids associated to the presence of a vertical structural limit visible in the resistivity tomography at the base of the edifice. This fault reaching more than 100 m b.s.l. could be attributed to the NNW regional volcano-tectonic orientation affecting the island of Vulcano.

(3) The former-crater rims, even when partially buried, remain preferential paths for hydrothermal fluid circulations as evidenced for the FV, PN, and Pa craters, which are underlined by strong temperature and CO_2 degassing anomalies and associated with low resistivity values at depth.

Circulations of hydrothermal fluids have been evidenced at the base of the north-western flank, by a variation of temperature of ~6°C from the south-east to the north-west along the profile 4. Such a distal anomaly of temperature can be due either to rising hydrothermal fluids or to fluids contaminated by the hydrothermal release in the summit area and flowing down to the base into shallow ground levels of the north-western flank. The north-western end of Profile 4 could be a relevant site for monitoring the temperature variations, if the fluctuations of the main hydrothermal system activity influence also the hydrothermal circulations at the base of the cone.

Our study also reveals the presence of an old magmatic body, dome or shallow intrusion, associated to the activity of the Punte Nere cone. The PC crater intersects this magma body on 200 m high, destructing its western part during the formation of the crater. The interface between the resistive body and the deposits filling the inner crater is one of the major structural limits of the edifice and constitute the eastern limit of the main hydrothermal system of La Fossa cone.

Acknowledgments. We thank Xavier Rassion for his help in the field. A special thanks to Maria Marsella for providing us the high resolution orthophoto and the digital elevation model of Vulcano Island. The INSU-CNRS, Istituto di Metodologie per l'Analisi Ambientale (IMAA) del CNR, the Laboratoire GéoSciences Réunion-IPGP, the CNR, the Istituto Nazionale di Geofisica e Vulcanologia (INGV), and the Dipartimento per la Protezione Civile through the DPC Projects (Sub-project V3.5 Vulcano, Agreement 2005-2007) are thanked for financial supports. We also thank Andrea Borgia for interesting discussions. This is IPGP contribution number: 2446. We thank the editor, Joan Marti, an anonymous referee, and Jean-François Lénat for their very useful comments on our manuscript.

References

Acocella, V., Cifelli, F., Funiciello, R., 2000. Analogue models of calderas and resurgent domes. J. Volcanol. Geotherm. Res. 104, 81-96.

Allard, P., Carbonnelle, J., Dajlevic, D., Le Bronec, J., Morel, P., Robe, M. C., Morenas, J.M., Faivre-Pierret, R., Martin, D., Sabroux, J.C., Zettwoog, P., 1991. Eruptive and diffuse emissions of CO_2 from Mount Etna. Nature 351, 387–391.

Anderson, E.M., 1936. The dynamics of the formation of cone sheets, ring dikes, and cauldron subsidences. Proceedings of the Royal Society of Edinburgh 56, 128–163.

Arrighi, S, Tanguy, J.-C., Rosi, M., 2006. Eruptions of the last 2200 years at Vulcano and Vulcanello (Aeolian Islands, Italy) dated by high accuracy archeomagnetism. Phys. Earth Planet. Int. 159, 225–233. doi:10.1016/j.pepi.2006.07.010

Aubert, M., Lima, E., 1986. Hydrothermal activity detected by self-potential measurements (SP) at the N-S volcanic axis between the volcanoes “Nevado de Colima” and “Fuego de Colima”, Mexico. Geophys. J. Int., 25-4: 575-586.

Aubert, M., Baubron, J.-C., 1988. Identification of a hidden thermal fissure in volcanic terrain, using a combination of hydrothermal convection indicators and soil-atmosphere analysis. J. Volcanol. Geotherm. Res. 35, 217-225.

Aubert, M., Diliberto, S., Finizola, A., Chébli, Y., 2007. Double origin of hydrothermal convective flux variations in the Fossa of Vulcano (Italy). Bull. Volc. doi 10.1007/s00445-007-0165-y

Auken, E., Christiansen, A. V., 2004. Layered and laterally constrained 2D inversion of resistivity data. Geophysics, 69, 752–761.

Barberi, F., Neri, G., Valenza, M., Villari, L., 1991. 1987–1990 unrest at Vulcano. Acta Vulcanol. 1, 95–106.

Barberi, F., Gandino, A., Gioncada, A., La Torre, P., Sbrana, A., Zenucchini, C., 1994. The deep structure of the Eolian Arc (Filicudi-Panarea-Vulcano sector) in light of gravimetric, magnetic and volcanological data. J. Volcanol. Geotherm. Res. 61, 189-206.

Baubron, J.C., Allard, P., Toutain, J.P., 1990. Diffuse volcanic emissions of carbon dioxyde from Vulcano Island, Italy. Nature 344, 51-53.

Bernard, M.-L., Zamora, M., Géraud, Y., Boudon, G., 2007. Transport properties of pyroclastic rocks from Montagne Pelée volcano (Martinique, Lesser Antilles). J. Geophys. Res. 112, B05205, doi:10.1029/2006JB004385.

Binley, A., Kemna, A., 2005. DC resistivity and induced polarization methods. In Hydrogeophysics, edited by Y. Rubin and S. Hubbard, chap. 5, pp. 129– 156, Springer, New York.

Blanco-Montenegro, I., de Ritis, R., Chiappini, M., 2007. Imaging and modelling the subsurface structure of volcanic calderas with high-resolution aeromagnetic data at Vulcano (Aeolian Islands, Italy). Bull. Volc. 69, 643-659. doi 10.1007/s00445-006-0100-7

Branney, M.J., 1995. Downsag and extension at calderas: new perspectives on collapse geometries from ice-melt, mining, and volcanic subsidence. Bull. Volcanol. 57, 303– 318.

Bukumirovic, T., Italiano, F., Nuccio, P.M., 1997. The evolution of a dynamic geological system: the support of a GIS for geochemical measurements at the fumarole field of Vulcano, Italy. J. Volcanol. Geotherm. Res. 79, 253-263.

Capasso, G., Favara, R., Inguaggiato, S., 1997. Chemical features and isotopic composition of gaseous manifestations on Vulcano Island, Aeolian Islands, Italy: An interpretative model of fluid circulation. Geochimica et Cosmochimica Acta vol. 61, No. 16, 3425-3440.

Capasso, G., Favara, R., Inguaggiato, S., 2000. Interaction between fumarolic gases and thermal groundwaters at Vulcano Island (Italy): evidences from chemical composition of dissolved gases in waters. J. Volcanol. Res. 102, 309-318.

Cecchi, E., Van Wyk de Vries, B., Lavest, J.-M., 2005. Flank spreading and collapse of weak-cored volcanoes. Bull. Volcanol. 67, 72–91.

Chébli, Y., 1997. Tomographie thermique et géoélectrique du cratère du Vulcano. Mémoire de D.E.A. Processus Magmatiques et Métamorphiques - Volcanologie, Université Blaise Pascal, Clermont-Ferrand II, 60 pp.

Chiodini, G., Cioni, R., Guidi, M., Marini, L., Raco, B., 1998. Soil CO_2 flux measurements in volcanic and geothermal areas. Appl. Geochem. 13, 543-552.

Day, S. J., 1996. Hydrothermal pore fluid pressure and the stability of porous, permeable volcano. In Volcano Instability o the Earth and Other Planets, McGuire W. J., Jones A. P., and Neuberg J. (Eds), Geol. Soc. Spec. Publ. 110, 77-93.

De Astis, G., Frazzetta, G., La Volpe, L., 1989. I depositi di riempimento della Caldera del Piano e i depositi della Lentia. Boll. G.N.V. 1989 (2), 763-778.

De Astis, G., La Volpe, L., Peccerillo, A., Civetta, L., 1997. Volcanological and petrological evolution of Vulcano island (Aeolian Arc, southern Tyrrhenian Sea). J. Geophys. Res. 102, B4, 8021–8050.

De Astis, G., Ventura, G., Vilardo, G., 2003. Geodynamic significance of the Aeolian volcanism (Southern Tyrrhenian Sea, Italy) in light of structural, seismological, and geochemical data. Tectonics 22, 4, 14.1–14.17.

De Astis, G., Dellino, P., La Volpe, L., Lucchi, F., Tranne, C.A., 2007. Geological map of the Vulcano Island, 1:10000, L. La Volpe & G. De Astis Eds.

Dellino, P, La Volpe, L., 1997. Stratigrafia, dinamiche eruttive e deposizionali, scenario eruttivo e valutazioni di pericolosità a La Fossa di vulcano. In : "CNR-GNV Progetto Vulcano 1993-1995" L. La Volpe, P. Dellino, M. Nuccio, E. Privitera, and A. Sbrana (Ed), Felici, Pisa, 214-237.

De Rosa, R., Calanchi, N., Dellino, P.F., Francalanci, L., Lucchi, F., Rosi, M., Rossi, P.L., Tranne, C.A., 2004. 32nd International Geological Congress, Field Trip Guide Book – P42, vol. n°5: Geology and volcanism of Stromboli, Lipari, and Vulcano (Aeolian Islands); Firenze 20-28 agosto 2004.

Durand, S., 1997. Etude structurale de la zone sommitale du Karthala (Grande Comore) par polarisation spontanée. Travail d'Etude et de Recherche. Univ. Blaise Pascal, Clermont-Ferrand II, 26 pp.

Finizola, A., Sortino, F., Lénat, J.-F., Valenza, M., 2002. Fluid circulation at Stromboli volcano (Aeolian Islands, Italy) from self potential and CO_2 surveys. J. Volcanol. Geotherm. Res. 116, 1-18.

Finizola, A., Sortino, F., Lénat, J-F., Aubert, M., Ripepe, M., Valenza, M., 2003. The summit hydrothermal system of Stromboli: New insights from self-potential, temperature, CO_2 and fumarolic fluids measurements, with structural and monitoring implications. Bull. Volcanol. 65, 486-504. doi:10.1007/s00445-003-0276-2

Finizola, A., Lénat, J.-F., Macedo, O., Ramos, D., Thouret, J.-C., Sortino, F., 2004. Fluid circulation and structural discontinuities inside Misti volcano (Peru) inferred from self-potential measurements. J. Volcanol. Geotherm. Res. 135, 343-360.

Finizola, A., Revil, A., Rizzo, E., Piscitelli, S., Ricci, T., Morin, J., Angeletti, B., Mocochain, L., Sortino, F., 2006. Hydrogeological insights at Stromboli volcano (Italy) from geoelectrical, temperature, and CO_2 soil degassing investigations. Geophys. Res. Lett. 33, L17304. doi: 10.1029/2006GL026842.

Frazzetta, G., La Volpe, L., Sheridan, M.F., 1983. Evolution of the Fossa cone, Vulcano. J. Volcanol. Geotherm. Res. 17, 329–360.

Frazzetta, G., Gillot, P.Y., La Volpe, L., Sheridan, M.F., 1984. Volcanic hazards at Fossa of Vulcano: data from the last 6000 years. Bull. Volcanol. 47, 105–124.

Ghisetti, F., 1979. Relazioni tra strutture e fasi trascorrenti e distensive lungo i sistemi Messina-Fiumefreddo, Tindari-Letojanni e Alia-Malvagna (Sicilia nord-orientale): uno studio microtettonico. Geol. Rom. 18, 23-56.

Granieri, D., Carapezza, M.L., Chiodini, G., Avino, R., Caliro, S., Ranaldi, M., Ricci, T., Tarchini, L., 2006. Correlated increase in CO_2 fumarolic content and diffuse emission from la Fossa crater (Vulcano, Italy): Evidence of volcanic unrest or increasing gas release from a stationary deep magma body ? Geophys. Res. Lett. 33, L13316. doi:10.1029/2006GL026460.

Griffiths, D.H., Barker, R.D., 1993. Two-dimensional resistivity imaging and modelling in areas of complex geology. J. Appl. Geophys. 29, 211-226.

Ishido, T., 2004. Electrokinetic mechanism for the "W"-shaped self-potential profile on volcanoes. Geophys. Res. Lett. 31, L15616, doi:10.1029/2004GL020409.

Keller, J., 1970. Die historischen eruptionen von Vulcano und Lipari, Zeit. Deut. Geol. Ges. 121, 179–185.

Keller, J., 1980. The island of Vulcano. Rend. Soc. Ital. Mineral. Petrol. 36, 369-414.

Lénat, J.F., Robineau, B., Durand, S., Bachèlery, P., 1998. Etude de la zone sommitale du volcan Karthala (Grande Comore) par polarisation spontanée. C. R. Acad. Sci. 327, 781–788.

Lo Cascio, P., Navarra, E., 1997. Guida Naturalistica Alle Isole Eolie. L'EPOS, Palermo. 112p.

Loke, M.H., 2004. Tutorial 2-D and 3-D electrical imaging surveys. Geotomo Software, Malaysia, 128p.

Loke, M.H., Barker, R.D., 1996. Rapid least-square inversion of apparent resistivity pseudosections by a quasi-Newton method. Geophys. Prospect. 44, 131-152.

López, D. L., Williams, S. N., 1993. Catastrophic volcanic collapse: relation to hydrothermal processes. Science 260, 1794-1796.

Malengreau, B., Lénat, J.-F., Bonneville, A., 1994. Cartographie et surveillance temporelle des anomalies de polarisation spontanee (PS) sur le Piton de la Fournaise: Cartography and temporal observation of self-potential (SP) anomalies at Piton de la Fournaise. Bull. Soc. Geol. Fr. 165(3), 221–232.

Mazzuoli, R., Tortorici, L., Ventura, G., 1995. Oblique rifting in Salina, Lipari and Vulcano islands (Aeolian islands, southern Italy). Terra Nova 7, 444-452.

Merle, O., Lénat, J.-F., 2003. Hybrid collapse mechanism at Piton de la Fournaise volcano, Reunion Island, Indian Ocean. J. Geophys. Res. 108, B3, 2166.

Michel, S., Zlotnicki, J., 1998. Self-potential and magnetic surveying of La Fournaise Volcano (Reunion Island): Correlations with faulting, fluid circulation, and eruption. J. Geophys. Res. 103, 17,845–17,857.

Montalto, A., 1994. Seismic signals in geothermal areas of active volcanism: a case study from "La Fossa", Vulcano (Italy). Bull. Volcanol. 56, 220–227.

Pribnow, D. F. C., Schütze, C., Hurter, S. J., Flechsig, C., Sass, J. H., 2003. Fluid flow in the resurgent dome of Long Valley Caldera: implications from thermal data and deep electrical sounding. J Volcanol Geotherm Res 127, 329-345

Rabaute, A., Revil, A., Brosse E., 2003. In situ mineralogy and permeability logs from downhole measurements. Application to a case study in clay-coated sandstone formations, J. Geophys. Res. 108, 2414. doi: 10.1029/2002JB002178.

Ramsey, M. S., Fink, J. H., 1999. Estimating silicic lava vesicularity with thermal remote sensing: a new technique for volcanic mapping and monitoring. Bull. Volc. 61, 32-39.

Reid, M. E., Sisson, T. W., Brien, D.L., 2001. Volcano collapse promoted by hydrothermal alteration and edifice shape, Mount Rainier, Washington. Geology 29, n° 9, 779-782.

Revil, A., Hermitte, D., Spangenberg, E., Cochémé, J. J., 2002. Electrical properties of zeolitized volcaniclastic materials. J. Geophys. Res. 107(B8), 2168. doi:10.1029/2001JB000599.

Revil, A., Finizola, A., Sortino, F., Ripepe, M., 2004. Geophysical investigations at Stromboli volcano, Italy: implications for ground water flow and paroxysmal activity. Geophys. J. Intern. 157, 426-440.

Revil, A., Finizola, A., Piscitelli, S., Rizzo, E., Ricci, T., Crespy, A., Angeletti, B., Balasco, M., Barde Cabusson, S., Bennati, L., Bolève, A., Byrdina, S., Carzaniga, N., Di Gangi, F., Morin, J., Perrone, A., Rossi, M., Roulleau, E., Suski, B., 2008. Inner structure of La Fossa di Vulcano (Vulcano Island, southern Tyrrhenian Sea, Italy) revealed by high-resolution electric resistivity tomography coupled with self-potential, temperature, and CO_2 diffuse degassing measurements. J. Geophys. Res. 113, B07207. doi:10.1029/2007JB005394.

Ricci, T., 2007. Studio del degassamento diffuso di CO_2 e indagini geofisiche a finalità idrogeologica nei vulcani attivi di Stromboli e de La Fossa di Vulcano: variazioni temporali e loro significato vulcanologico, implicazioni strutturali, per il monitoraggio geochimico e per la pericolosità da gas. Phd Thesis, Università di Roma Tre

Roberts, J. J., Lin, W., 1997. Electrical properties of partially saturated Topopah Spring tuff: Water distribution as a function of saturation, Water Resour. Res., 33, 577– 587.

Roche O., Druit T.H., Merle, O., 2000. Experimental study of caldera formation. J. Geophys. Res. 105, N°B1, 395-416

Roche, O., van Wyk de Vries, B., Druitt, T.H., 2001. Sub-surface structures and collapse mechanisms of summit pit craters. J. Volcanol. Geotherm. Res. 105, 1-18

Vallance, J. W., Scott, K. M., 1997. The Osceola Mudflow from Mont Rainier: Sedimentology and hazard implications of a huge clay-rich debris flow. GSA Bulletin 109, n° 2, 143–163.

Van Wyk de Vries, B., Kerle, N., Petley, D., 2000. Sector collapse forming at Casita volcano, Nicaragua. Geology 28, n° 2, 167-170.

Ventura, G., 1994. Tectonics, structural evolution and caldera formation on Vulcano Island (Aeolian Archipelago, southern Tyrrhenian Sea). J. Volcanol. Geotherm. Res. 60, 207-224.

Ventura, G., Vilardo, G., Milano, G., Pino, N. A., 1999. Relationships among crustal structure, volcanism and strike-slip tectonics in the Lipari-Vulcano Volcanic Complex (Aeolian Islands, Southern Tyrrhenian Sea, Italy). Phys. Earth Planet Int., Volume 116, Issue 1-4, 31-52.

Voight, B., Elsworth, D., 1997. Failure of volcano slope. Géotechnique 47(1), 1-31.

Walter, T.R., Troll, V.R., 2001. Formation of caldera periphery faults: an experimental study. Bull. Volc. 63, 191-203.

Wohletz, K., Heiken, G., 1992. Volcanology and geothermal energy. J.H. Heiken (Ed.), University of California Press., 432p.

Zablocki, C.J., 1976. Mapping thermal anomalies on an active volcano by the self-potential method, Kilauea, Hawaii. Proceedings, 2nd U.N. Symposium on the development and use of geothermal resources, San Francisco, California, May 1975, 2, 1299-1309.

Figure captions:

Figure 1. Location of the studied area. Simplified geological map of La Fossa cone draped on the DEM (map simplified from de Astis et al., 2007) and chronology. PN (Punte Nere), Pa (Palizzi), FV (Forgia Vecchia), PC (Pietre Cotte), and GC (Gran Cratere) crater rims are represented. In the upper right corner, Vu, VP, and LFc stand for Vulcanello, Vulcano Primordiale and La Fossa cone. On the location and structural sketch map of the Aeolian Islands area M, AI, TL, and ME stand for the Marsili Oceanic Basin, the Aeolian Islands represented by white ellipses (red star for Vulcano; black shapes for seamounts), the Tindari-Letojanni fault system, and the Malta Escarpment fault system (sketch simplified from Ventura et al., 1999).

Figure 2. Location of the 9 profiles performed, on the orthophotography overlaid on the DEM of La Fossa cone. Bright orange profiles are those detailed in the text. White dots represent the measure points. The light pink areas on the flanks of the volcano correspond to the hydromagmatic tuff discussed in the main text.

Figure 3. Temperature, Self potential, and soil CO_2 flux maps of La Fossa cone, interpolated from the data of the nine profiles performed, overlaid on the DEM. White and black dots represent the measure points. PN (Punte Nere), Pa (Palizzi), FV (Forgia Vecchia), PC (Pietre Cotte), and GC (Gran Cratere) craters are localised with white dashed lines.

Figure 4. Temperature, self-potential, soil CO_2 flux, and electric resistivity tomography along Profile 1. Note the sharp resistivity transition on the GC crater boundaries. PN: Punte Nere crater, PC: Pietre Cotte crater, GC: Gran Cratere crater.

Figure 5. Temperature, self-potential, soil CO_2 flux, and electric resistivity tomography along profile 4. Note the sharp resistivity transition (black arrow) at a distance of 2000 m underlined by a temperature and soil CO_2 flux maximum. The black arrow is also localized on map in Figure 6.

Figure 6. Map representation of the temperature variation at the base of the cone, along profile 4. White dots represent the measure points. The black arrow is pointing the resistivity transition highlighted by electrical resistivity tomography (see figure 5).

Figure 7. Temperature, self-potential, soil CO_2 flux, and electric resistivity tomography along profile 6. Note the correspondence of the temperature, self-potential, and soil CO_2 flux anomalies with low values of resistivities reaching the surface. PN: Punte Nere crater, PC: Pietre Cotte crater, GC: Gran Cratere crater, F: fumaroles.

Figure 8. Temperature, self-potential, soil CO_2 flux, and electric resistivity tomography along profile 8. Note the presence of a large resistive body under the Punte Nere former cone (see also profile 1 on figure 4). PN: Punte Nere crater, PC: Pietre Cotte crater, GC: Gran Cratere crater.

Figure 9. a. Image map of the electrical resistive body draped on the DEM; b. 3D view of the resistive body under a truncated DEM of La Fossa; c. 3D view of the resistive body from the south-east. The colour scale represents the elevation of the surface of the resistive body. Only the measured points used to build the 3D representation of the resistive body are visible (black and white dots). PN: Punte Nere, Pa: Palizzi, FV: Forgia Vecchia, PC: Pietre Cotte, and GC: Gran Cratere. Coordinates are in meter, UTM (WGS84).

Figure 10. Schematic representation of the evolution of the cone, from Punte Nere to nowadays. The information on both the geology and on the fluid circulation is shown. The synthetic sketch is based on Profile 8. PN: Punte Nere crater, PC: Pietre Cotte crater, GC: Gran Cratere crater.

New geological insights and structural control on fluid circulation in La Fossa cone (Vulcano, Aeolian Islands, Italy)

Barde Cabusson S. (1, 2), Finizola A. (3, 4), Revil A. (5, 6, 7), Ricci T. (8), Piscitelli S. (9), Rizzo E. (9), Angeletti B. (6), Balasco M. (9), Bennati L. (10), Byrdina S. (2, 11), Carzaniga N. (12), Crespy A. (6), Di Gangi F. (4), Morin J. (3, 13), Perrone A. (9), Rossi M. (14, 12), Roulleau E. (15), Suski B. (16, 6), Villeneuve N. (17)

(1) Dipartimento di Scienze della Terra, Università Degli Studi di Firenze, Italy
(2) LMV, Université Blaise Pascal, Clermont-Ferrand, France
(3) Laboratoire GéoSciences Réunion, UR, IPGP, UMR 7154, Saint-Denis, La Réunion, France
(4) Istituto Nazionale di Geofisica e Vulcanologia, Palermo, Italy
(5) Colorado School of Mines, Dept. of Geophysics, Golden, CO, USA
(6) CNRS-CEREGE, Université Paul Cézanne, Aix en Provence, France
(7) CNRS-LGIT (UMR 5559), University of Savoie, Equipe Volcan, Chambéry, France
(8) Istituto Nazionale di Geofisica e Vulcanologia, Roma, Italy
(9) IMAA-CNR, Laboratory of Geophysics Tito Scalo (PZ), Italy
(10) Dept. of Earth & Atmospheric Sciences, Purdue University, West Lafayette, USA
(11) Equipe de Géomagnétisme, IPGP, UMR 7154, 4, Place Jussieu, 75005 Paris, France
(12) Università Milano-Bicocca, Milan, Italy
(13) Université Paris 1, Panthéon-Sorbonne, Paris, France
(14) Dipartimento di Geoscienze, Università di Padova, Italy
(15) GEOTOP-UQAM-McGill, Montréal, Canada
(16) Université de Lausanne (UNIL), Institut de Géophysique, Lausanne, Switzerland
(17) Institut de Recherche pour le Développement, US 140 ESPACE, La Réunion, France

---

Corresponding author :

Stéphanie Barde-Cabusson (Dipartimento di Scienze della Terra, Università di Firenze, Via Giorgio La Pira 4, 50121, Firenze, Italy; email : s.barde.cabusson@gmail.com; Tel. +39-055-2757479 ; Fax +39-055-2756242)

Abstract

Electric resistivity tomography (ERT), self-potential (SP), soil CO_2 flux, and temperature are used to study ~~provide detailed information about~~ the inner structure of La Fossa cone (Vulcano, Aeolian Islands). Nine profiles were performed across ~~through~~ the cone with a measurement spacing of 20 m. The crater rims of La Fossa cone are underlined by sharp horizontal ~~transitions of~~ resistivity contrasts ~~displayed by the ERT sections~~. SP, CO_2 flux, and temperature anomalies underline ~~highlight~~ these boundaries which we interpret as structural limits ~~are~~ associated to preferential circulation of fluids. The Pietre Cotte crater and Gran Cratere craters enclose the main hydrothermal system, identified at the centre of the edifice ~~by~~ on the base of low ~~values of the~~ electrical resistivity values (< 20 Ω.m) and strong CO_2 degassing, SP, and temperature anomalies. In the periphery, the hydrothermal activity is also visible along structural boundaries such as the Punte Nere, Forgia Vecchia, and Palizzi crater rims and at the base of the cone, on the southern side of the edifice, along a fault attributed to the NW main tectonic trend of the island. Inside the Punte Nere crater, the ERT sections show an electrical resistive body that we interpret as an intrusion or a dome. This magmatic body is reconstructed in 3D using the available ERT profiles. Its shape and position, with respect to the Pietre Cotte crater fault, allows replacing this structure in the chronology of the development of the ~~this~~ volcano. It corresponds to a late phase of activity of the Punte Nere edifice. Considering the position of the SP, soil CO_2 flux, and temperature maxima and the repartition of conductive zones related to hydrothermal circulation with respect to the main structural features, La Fossa cone could be considered as a relevant example of the strong influence of pre-existing structures on hydrothermal fluid circulation at the scale of a volcanic edifice.

Keywords: Electrical resistivity; self-potential; soil CO_2 degassing; temperature; fluid circulation; hydrothermal system; structural boundary; Vulcano; La Fossa cone.

Short title: Structural control on fluid circulation

1. Introduction

Active volcanoes are not only the place of magma~~tic~~ transfers but also of permanent heat and fluid transfers from the magma~~tic~~ reservoir to the ~~ground~~ surface, even during long periods of eruptive quiescence. These exchanges are mainly insured by convective circulations of hot ground fluids (gas and liquids) inside the hydrothermal system (e.g., Aubert and Baubron, 1988; Granieri et al., 2006; Finizola et al., 2003, 2006).

A volcanic edifice can be a very heterogeneous structure due to its eruptive dynamics and evolution. It is usually shaped by an alternation of lava flow units, ash layers, volcanoclastic deposits, clay-rich materials resulting from hydrothermal alteration, various intrusions, all heterogeneously affected by deformation and the presence of cracks. During its evolution, more ~~or less~~ permeable levels and interfaces develop ~~between~~ owing to the superposition of the various geological units ~~showing contrasted rheological behaviours. These interfaces can sometimes constitute zones of weakness favourable to fluid circulation through the edifice.~~ However, structural limits and fracture zones formed inside the volcano along its history can constitute the more permeable zones. These weakness planes allow the infiltration of meteoric waters, the rise of hydrothermal fluids, and sometimes the transfer of magma. ~~They are likely the main paths for magma transfers as well as for descending meteoric waters and rising hydrothermal fluids.~~ A good example is provided by caldera structures, where the hydrothermal activity concentrates along the border fault and on intracalderic fractures (e.g., Pribnow et al., 2003). In a comparative study of the Valles caldera (New Mexico) and of the calderas of Lake City and Platoro (Colorado), Wohletz and Heiken (1992) highlights that the hydrothermal alteration develops principally along the faults formed inside the caldera and around shallow intrusions. Also, the craters boundaries ~~are very similar structures and~~ being highly permeable zones of the edifice, they usually guide fluid circulation in the same way (e.g., Revil et al., 2004). In addition to these localized pathways, the transfers can be ~~also~~ more pervasive depending on the permeability of the volcanic materials, e.g., the diffuse degassing of CO_2 (Baubron et al., 1990; Allard et al., 1991).

The hydrothermal activity can also alter the cohesion of rocks and therefore be responsible for large collapses and landslides or for ~~favouring~~ the spreading of ~~the~~ volcanic edifices (Lopez and Williams, 1993; Day, 1996; Vallance and Scott, 1997; Voight and Elsworth, 1997; van Wyk de Vries et al., 2000; Reid et al., 2001; Cecchi et al., 2005; Merle and Lénat, 2003). The hydrothermal alteration, in addition to increasing ~~increases~~ the risk of instability, ~~of a volcanic edifice and~~ also enhances the mobility of the debris avalanches.

Indeed, the hydrothermal alteration reduces the cohesion of the rock and increases the fluid content favouring these risks ~~depending on the fluid content of the rock and their cohesion~~ (e.g., Vallance and Scott 1997). On Vulcano, ~~the last~~ a ~~major~~ landslide occurred the 20th April 1988 on the north-eastern flank of La Fossa cone. A volume of 220.000 m^3 of superficial pyroclastic deposits was implicated. ~~One hypothesis for to explain is~~ This destabilization was contemporary of the opening of fractures affected by fumarolic emanations and hydrothermal alteration ~~and new fractures in the summit area~~ (Ricci, 2007). Currently, given the strong alteration of the rocks around the Forgia Vecchia (north-north-east flank) this area is of major landslide-probability and, due to the population density, in particular during the tourist season, it presents a major risk ~~is located under the Forgia Vecchia crater~~. Understanding the relationships between pre-existing structures and fluid circulation is ~~an~~ important ~~approach~~ to study volcanic hydrothermal systems and could help to forecast possible volcanic instabilities in the long term.

Because drilling volcanic edifices is difficult, non-intrusive methods that can image the structure of a volcanic edifice and that can be sensitive to the flow of the ground water and CO_2 are important to understand the dynamics of hydrothermal systems. They constitute ~~can be considered as~~ very important tools to extrapolate the observations made at the ground surface to depth in order to draw a map of the geohazards associated with a volcanic edifice. La Fossa cone (Vulcano, Aeolian Islands, Italy) is a small and complex volcanic edifice characterized by a strong alteration due to a very active hydrothermal system. In addition, we have a good knowledge regarding its eruptive history (De Astis et al., 2007 and references therein). It is therefore an ideal ~~perfect~~ natural laboratory to conduct a high resolution survey investigating the structure and the hydrothermal system of a volcanic edifice.

We acquired ~~data in~~ multi-electrode electric resistivity data ~~tomography~~ (ERT), self potential (SP), soil CO_2 diffuse degassing, and shallow ground temperature data along several profiles. The same dataset was used by Revil et al. (2008) to present the main structural features interpreted from some of the profiles and to perform a numerical modelling of the ground water flow pattern. In our case, this multidisciplinary ~~approach~~ study is used to map the ~~surface~~ signature of the hydrothermal activity of La Fossa cone and to ~~reveal~~ detail its inner structure above the sea level.

The main goals of this study are (1) to interpret the data in terms of geological features and (2) to understand how pre-existing geological structures control the pattern of fluid circulation.

2. Geological setting

Located in the south of Tyrrhenian Basin, Vulcano is the third largest of the seven Aeolian Islands. It is also the southernmost island of the archipelago. Salina, Lipari, and Vulcano are three islands ~~that present~~ aligned along a NNW-SSE trend, unconformable with respect to the arc layout. This volcanic lineament ~~characteristic~~ is explained by a magmatic activity controlled by regional tectonics. Indeed, the development of these islands is strongly influenced by an active crustal discontinuity related to the Tindari-Letojanni dextral strike-slip fault system formed in the continuation of the Malta escarpment (Barberi et al., 1994; Ventura, 1994; Ghisetti, 1979). The horizontal displacements along the strike-slip system are accommodated by N-S to NE-SW trending normal faults and accompanied by pure extension (Mazzuoli et al., 1995).

Vulcano Island was built by a succession of constructive and destructive stages ~~undergone by~~ of the two main edifices, ~~which are~~ Vulcano Primordiale and La Fossa cone (Fig. 1). Vulcano Primordiale is the oldest (120-100 ka, see Keller, 1980). This unit, located in the southern part on the island, is also commonly named Piano or Serro di Punta Lunga. This stratovolcano has been truncated around 100 ka by the collapse of the Piano Caldera, now filled by post-collapse eruptive materials (De Astis et al., 1989). The eruptive centre has then migrated to the north-west to form the Cardo tuff cone and the Lentia intrusive Complex. Both have been largely masked owing to ~~This edifice is almost totally invisible nowadays because of~~ the collapse of La Fossa Caldera and because of the edification of La Fossa cone inside the caldera depression (De Astis et al., 2007).

La Fossa cone is a 391 m height stratocone, active since ~6000 years (Dellino and La Volpe, 1997; De Rosa et al., 2004). Its eruptive history and structure have been studied by many authors (e.g., Keller, 1970, 1980; Frazzetta et al., 1983, 1984; Dellino and La Volpe 1997; De Astis et al., 1997, 2003, Arrighi et al., 2006). The present day ~~actual~~ edifice results from six main phases of activity described in the last issue ~~update~~ of the geological map of the island (De Astis et al., 2007) which we simplified in Figure 1.

(1) Punte Nere formation is composed of pyroclastic products corresponding to surges and fallouts deposits at the base. The upper unit is a succession of aa lava flows. This ~~first~~ formation constitutes the former Fossa cone, associated to Punte Nere crater (PN) and now truncated to the west by the ~~actual active~~ younger cone.

(2) Palizzi formation is composed of three units. The first unit show a pyroclastic succession of varicoloured ashes (“Tufi varicolori di La Fossa”). Two younger units display an alternation of pyroclastic deposits and lava flows. In the meantime, a new eruptive centre was active in the northern part of the island, forming the Vulcanello peninsula. The corresponding crater rim (Pa) is nowadays only visible on the southern part of La Fossa cone.
(3) Caruggi formation, previously named Commenda (Frazzetta et al., 1984; Arrighi et al., 2006) consists of pyroclastic deposits with yellow-reddish ashes and rounded, hydrothermalized lithic blocks. The upper unit corresponds to varicoloured tuffs and ash layers. This layer is well recognized in the landscape as pink coloured outcrops ~~(see Figure 2)~~.
(4) Forgia Vecchia formation has settled on the northern flank of La Fossa cone and is made up of lahar deposits. This stage also left an adventive crater (FV), approximately 300 m wide, on the northern flank.
(5) Pietre Cotte formation consists of a pyroclastic unit mainly visible on the southern flank of La Fossa cone. The cycle is ended by the emission of a striking tongue-like rhyolitic lava flow easily recognisable on the northwest flank. The corresponding crater of Pietre Cotte stage (PC) intersects both PN and Pa craters.
(6) Gran Cratere formation is a pyroclastic level clearly visible on the major part of La Fossa cone as grey ashes. This stage of activity ended with the historical 1888-1890 eruption and gave rise to the formation of a succession of nested craters (GC) partly overlapping the PC crater rim.

The current activity on Vulcano is characterized by intense fumarolic emissions in La Fossa crater, on the northern and southern flanks of the edifice and in the area of the ~~areas of Faraglione, Spaggia di Levante and,~~ Porto di Levante harbour. Other isolated fumaroles have been observed on the flanks of the edifice while a strong cold degassing is localized in the Palizzi area. Since 1890 the quiescent La Fossa volcano is characterized by the occurrence of “crises” (Granieri et al., 2006) with strong increases of the fumaroles temperatures and output and variations of the chemical compositions toward more magmatic signatures caused by the uprising of magmatic gas. Moreover, a local anomalous shallow seismicity characterized by swarms of low-magnitude, due to rising gases in the fumarolic feeding system, an increase of the diffuse soil CO_2 degassing, and a spatial expansion of the fumarolic fields are also characteristic of these “crises” ~~Thermal and seismic crises disrupting the hydrothermal system are also occasionally registered. The last occurred in 2004-2006 (Granieri et al., 2006; Aubert et al., 2007)~~ but no evidence of magma uprising was signaled.

3. Data acquisition and processing

In October 2005, May 2006 and October 2006 we performed three multidisciplinary surveys. Nine profiles were deployed crossing the entire edifice, for a total length of 18980 m (Fig. 2). We acquired multi-electrode electrical resistivity data with an electrode spacing of 20 m. Self potential, CO_2, and temperature measurements were acquired on the same points ~~together with the other methods~~, which represent 957 measurements for these methods. ~~the self-potential, for the soil CO_2 flux as well as for the temperature measurements.~~ The ~~different~~ methods used during the surveys are described in detail in Revil et al. (2008). We ~~just~~ summarize the main points here:

3.1. Electric resistivity tomography

~~(1)~~ Resistivity measurements were acquired with an ABEM (SAS4000) resistivimeter with a multichannel system of 64 electrodes ~~device~~ connected to the acquisition system through a 1260 m long cable. We used a Wenner array because of its good signal-to-noise ratio ~~and the electrode spacing was 20 m~~. We added salty water around each electrode to decrease the contact resistance between the electrodes and the ground. Two or three roll-along~~s of the electrodes~~ were performed to complete each profile. The apparent resistivity values obtained were inverted by RES2DINV software (Geotomo software; Griffiths and Barker, 1993; Loke and Barker, 1996) obtaining a resistivity model along each section. Revil et al. (2008) detailed the inversion process and discussed the results of the tests run to check the uncertainty associated with the resistivity data. The authors conclude that the inverse modelling used is very robust to the noise existing in the raw data. The results allow visualizing a model of resistivity of the edifice. Some of the most representative resistivity models will be presented below as 2D cross-sections.

The interpretation of inverted data alone is a notoriously difficult task because electrical resistivity varies with a number of parameters including temperature, salinity, clay and zeolite contents and mineralogy, grain shape, and porosity (Revil et al., 2002; Rabaute et al., 2003). For the same data set, there are several possible resistivity models that fit the data equally well (e.g., Auken and Christiansen, 2004; Binley and Kemna, 2005). However, the resistivity models highlight clear spatial resistivity contrasts ~~mediums with different electrical resistivity values~~ that can be~~, in turn,~~ interpreted in terms of ~~different~~ lithology transitions.

3.2. Self potential

~~(2)~~ SP ~~Self-potential~~ measurements were performed using a pair of non-polarizing $Cu/CuSO_4$ electrodes. The difference of electrical potential between the reference electrode (conventionally placed at the beginning of the profile) and the scanning electrode was measured with a calibrated high impedance voltmeter with a sensitivity of 0.1 mV. The SP ~~self-potential~~ method ~~also~~ allows to map rising hydrothermal fluids on active volcanoes; e.g., on Kilauea in Hawaii (Zablocki, 1976), on Nevado de Colima and Fuego de Colima in Mexico (Aubert and Lima, 1986) ~~Etna in Italy (Aubert and Kieffer, 1984),~~ on Piton de la Fournaise in Reunion Island (Malengreau et al., 1994 and Michel and Zlotnicki, 1998), on the Karthala in Comoros (Durand, 1997; Lénat et al., 1998), on Stromboli in Italy (Finizola et al., 2002), and on Misti volcano in Peru (Finizola et al., 2004). ~~Recent developments allow using this information to map in 3D the pattern of ground water flow (Jardani et al., 2007, 2008; Straface et al., 2007).~~ In the present case, this method was useful to highlight the structural limits, which are usually preferential paths for ground water circulation and to map the hydrothermal activity.

3.3. Soil CO_2 flux

~~(3)~~ Soil CO_2 flux measurements were acquired using the methodology described by Chiodini et al. (1998). The instrumentation consists of an IR spectrometer Licor LI800 ~~to measure soil CO_2 fluxes from~~ with a range of 0 to 2000 µmol/mol (2 % vol.), an accumulation chamber (type A: ~~dead~~ volume of 30 cm^3) and a palmtop to plot the CO_2 increase as a function of time. The accumulation chamber is leaned on the ground so that the atmospheric air cannot penetrate inside. The gas permeating from the soil accumulates in the dead volume, passes through the IR spectrometer and is re-injected in the accumulation chamber. The increase of the concentration in the chamber through time allows determining the flux of CO_2 from the soil. This is a powerful method to detect preferential hydrothermal flux paths on a volcanic edifice. ~~These measurements provide information about the preferential flowpaths for CO_2 through the edifice.~~

3.4. Temperature at 30 cm depth

~~(4)~~ Temperature measurements were performed at a depth of 30 cm ± 1 cm and respecting a stabilisation time of 15 minutes. We used ~~using~~ thermal probes and a digital thermometer with a sensitivity of 0.1°C. The maximum amplitude of diurnal variation at Vulcano at 30 cm depth during the summer season is less than 1.2°C (Chébli, 1997; Aubert et al., 2007). During the year, at that depth, the temperature varies from 12.2 to 27.2°C in January and August, respectively (Lo Cascio and Navarra, 1997). Consequently, for measurements performed at 30 cm depth, we consider a temperature above 30°C as a signature of hydrothermal fluid circulations.

We made a ~~The~~ temperature map ~~is~~ interpolated from the data of the nine profiles (Fig. 3a). The data have been acquired within one year so that the amplitude of the thermal anomalies probably varied along the period of acquisition of the dataset due to seasonal and internal variations. However this figure gives reliable qualitative information ~~the location of the main anomalies remains the same~~. ***(Note from the authors**: these lasts three sentences were removed from the former-manuscript section 4.1. Temperature map)*

4. Results

4.1. Reliability of the temperature, CO_2, and SP maps

A map is supposed to present the state of a particular area within a short period of time, which suggests that the conditions along the acquisition of a dataset must remain relatively stable. Our dataset contains data from three surveys performed in a one year period (from October 2005 to October 2006). Concerning the SP measurements, we added a few data from a survey of 2004 (black dots on Figure 3b) in order to join the profiles to the sea, calculate a closure offset and distribute linearly this offset on the profiles to correct the global dataset presented here. Knowing that, we must take into account that some parameters influencing the measurements have undergone some variations, which can distort the maps. These parameters are the volcanic activity, the soil characteristics and the atmospheric conditions.

It seems that the temperature measurements at 30 cm depth are less affected by the variations undergone between our three surveys. It is true since the measurements are not performed during rain events. In fact the rain makes the temperature fall down of several degrees depending on the depth of infiltration of the meteoric water and the atmospheric temperature.

For the SP map, some strong positive and negative anomalies remain uncorrelated with the other methods and the main information is displayed in the PC/GC crater area and the PN crater. Variations of the volcanic activity, seasonal variations of the soil moisture are the possible responsible of some of the unexplained anomalies. The contrasts of resistivity of the terrain can also affect the SP measurements without affecting the CO_2 and temperature values.

The values of the soil diffuse degassing at La Fossa volcano during the last crisis, begun at the end of 2004, revealed fluctuations of CO_2 flux until one order of magnitude (Granieri et al., 2006). It was characterized by significant variations in the extension of the anomalous degassing area. The CO_2 flux data presented in this paper were collected in three different periods during the last crisis of La Fossa volcano. Consequently, the resulting CO_2 map of the entire La Fossa cone shown in Figure 3c is purely indicative because of the fluctuations in the degassing activity and no quantitative analyses can be done. Nevertheless the CO_2 map closely reflects the shape of the anomalous degassing areas presented by Granieri et al. (2006).

Finally, more than giving quantitative information, the temperature, SP, and CO_2 maps are useful to get qualitative information, i.e. structural information and a distribution of the hydrothermal emissions. Based on the correlations between these maps, several areas of interest have been identified and will be commented below.

4.2. The central hydrothermal system ~~Temperature map~~

In an interpolated map, the less the profiles are spaced, the more the interpolation is reliable so that, on the temperature, SP, and CO_2 maps, the most relevant information is concentrated around the data points (white and black dots on Figure 3). The most striking information provided by the global temperature map (Figure 3a) is that the main thermal ~~release zone~~ anomaly is bounded by the rim of the GC and PC craters, which are the most recent craters formed on La Fossa cone. This central thermal anomaly is correlated to anomalies of similar extension in SP and soil CO_2 flux (maps in Figure 3b and 3c).

The highest temperatures have been measured into the inner crater. Gases escape from the fumaroles at high temperature (~400°C) and ~~but~~, for the safety of the measuring devices, no measurement was made right on it. In the north-east area, the ~~strongest~~ thermal, SP and CO_2 anomalies extend beyond the GC rim, between the GC and the PC crater rims. In the field, these zones correspond to strong fumarolic activity and/or extensive hydrothermal alteration. The main fumarolic field is indeed located on the northern wall of the GC crater, on the rim, and extends beyond its limits (see Bukumirovic et al., 1997). On Vulcano, the temperatures of the fumaroles can reach several hundred degrees Celsius (almost 700°C during the 1977 crisis, see Barberi et al., 1991). Except on these particular locations, no measurement of our surveys overtakes 98°C. This can be explained by the presence, at depth, of a hot aquifer or of a shallow condensation zone formed under a sealed layer, acting as a thermal buffer between the magmatic heat source and the surface (Montalto 1994; Aubert et al., 2007). ~~Where a level saturated with liquid water exists at depth, the temperature above this depth cannot exceed the boiling point of water at that elevation.~~

These main thermal, SP, and CO_2 anomalies are the expression of the central active hydrothermal system activity and the data show that this hydrothermal system is bounded by the PC and GC crater faults.

4.3. Hydrothermal circulations along former structural limits

Hydrothermal fluid circulation is not restricted to the central crater area. Outside of the main Fossa craters area, we also identified few temperature, SP, and CO_2 anomalies. ~~This clearly indicates that fluid circulation is not restricted to the central crater area.~~ Not far from the central hydrothermal system, strong ~~temperatures~~ anomalies have been observed beyond the PC crater rim, on the northwest upper flank of the cone, right on the former footpath to the summit (see the central part of profile 2 in Figure 3). These high temperatures, SP, and CO_2 values are associated with fumarolic emissions~~, which was the reason for creating a new access to La Fossa crater for visitors~~.

4.3.1 Forgia Vecchia crater

On the northern flank, the Forgia Vecchia crater (FV) is affected by a thermal anomaly on its northern border (see northern section of Profile 3 on Figure 3a). The temperature measured is ~10°C above the mean temperature in this area. This is the only sign of current activity on this adventive crater, in our dataset. The FV crater border is a permeable limit acting as a guide for fluid circulation. The thermal release noticed here can be due to the presence, at shallow depth, of a still cooling magmatic batch related to the past activity. Another source could be distal hot fluid circulations associated to the current hydrothermal system of La Fossa cone.

4.3.2 Palizzi crater

On the southern flank of the edifice, Profiles 3, 5, and 6 display thermal and CO_2 anomalies on their intersection with the Pa crater rim. This crater rim is clearly underlined, even when the topography gives no evidence for it. The location of the anomalies coincides with the crater drawn by De Astis et al. (2007) in their geological map of Vulcano.

4.3.3 Punte Nere crater

One striking result is the observation of high temperature, SP, and CO_2 values in the area enclosed by the Punte Nere crater (PN), where no eruptive activity took place since 3.8 ka (De Astis et al., 2007). As shown by the data along the two profiles crossing the rim in the North (Profile 6) and in the East (Profile 8), the thermal and CO_2 anomalies extend outside the PN crater, on the upper part of the slope of the cone.

Two types of thermal anomalies can be distinguished in this area, which are (1) strong anomalies (in the range between 35°C and 60°C) along structural limits and (2) weak anomalies (smaller than 35°C) in areas poorly or unaffected by faulting. On Profiles 6 and 8, the temperature anomalies show that hydrothermal fluids take advantage of the high permeability along the crater rim to reach the ground surface. The maximum temperature registered is ~60°C. In this case, the heat can come from a deep source and produce strong anomalies in the vicinity of the ground surface. Concerning the wide anomalous temperature field inside the PN crater, temperatures reach a maximum of 35°C.

As for the FV crater but to a wider scale, the PN crater anomaly can have two potential origins: the ~~heat~~ hot-fluid source can be due either to circulations of fluids from La Fossa hydrothermal system or to remnants of the past activity of the Punte Nere cone. Profile 1 can help determining the source (Fig. 4). As on the maps (Fig. 3), an overview of this profile shows high values of temperature, self-potential, and CO_2 in the central part of the edifice. The self-potential data display a typical W shape (e.g., Ishido, 2004), confirming that the main hydrothermal activity is ~~then~~ concentrated in the limits of the GC crater. Crossing the eastern side of the GC crater rim, the temperature and CO_2 progressively decrease from west to east, inside the PN crater. The anomaly vanishes to reach characteristic temperatures of "cold" zones on the flank of the edifice. At depth, the resistivity structure shows a continuous conductive zone from the most internal crater to the flank of the cone. In the limits of the PC crater, the low resistivity is associated to the hydrothermal system, i.e. hydrothermal fluids convecting through the detritic volcanic deposits of the last phases of eruptive ~~volcanic~~ activity. Beyond the PC crater, we interpret the low resistivity layer as tuff deposits from La Fossa activity. The resistive body visible at depth acts as an impermeable limit so that the fluids are guided inside the more permeable overlying tuff level. Underground, the hot fluids rising from the central zone overflow to the east into the PN crater and progressively loose gases and heat. The temperature, SP, and CO_2 anomalies visible inside the PN crater can be attributed to this phenomenon, even if a contribution of a residual degassing activity of the PN volcanic centre cannot be ruled out.

4.4.2. Regional faulting evidences in the Palizzi area ~~Signal comparison at the base of the cone~~

Profile 4 was performed at the base of the cone, from Porto di Levante to an area situated to the East of Palizzi, near the Rio Grande bed. The CO_2 map (Fig. 3c) shows remarkable anomalies in the Palizzi area. The global temperature map (Fig. 3a) does not display a perceptible anomaly along Profile 4. However, a closer inspection of the data indicates a variation of ~6°C from one extremity of the profile to the other (see Figures 5 and 6). At the south-eastern end of the profile, the temperature is ~18°C. Following the profile to Porto di Levante, the temperature increases progressively and reaches a maximum of ~24°C. The data were acquired in only two days and with similar dry meteorological conditions all along this period of time. Moreover, this progressive temperature increase of ~6°C from the southern flank to the north-western flank of La Fossa cone exceeds the maximum amplitude of diurnal variation which is less than 1.2°C at Vulcano, for measurements performed at 30 cm depth during summer season (Chébli, 1997; Aubert et al., 2007). This makes of these 6°C ~~gradient~~ a significant variation.

In the northern and southern parts of the profile, the ERT model shows a shallow resistive layer associated to pyroclastic deposits. These deposits are from the Gran Cratere phase of activity in the northern portion of the profile and from the Palizzi phase in the south. This resistive layer of a few meters-thick overlays a low-resistivity medium (< 20 Ω.m). At the center of the profile, we notice the presence of a high resistivity zone. The thickness of this body globally increases from north to south. This structure is bounded by two vertical limits evidenced by sharp transitions of the resistivity. The northern boundary is rapidly blurring at depth. The southern boundary is marked by a sharpest transition of resistivity and runs from the shallow levels of the section, until the maximum depth of investigation.

On the northern part of the profile, the soil CO_2 flux decreases from north to south consistently with the global decrease of temperature observed along the whole profile. In the vicinity of the resistive body, the CO_2 flux increases, reaching a maximum in the area surrounding the southern vertical limit identified from the resistivity data. On the area surrounding the resistive body the short wave-length variations of the temperature are significantly lower than on the rest of the profile. Thereby, along our profile, the southern vertical limit of the resistive body marks a sharp increase of ~2.5°C of the mean temperature from north to south. Right on the northern boundary of the body, we also observe a slight soil CO_2 flux anomaly (~80 g/m².d) and a decrease of the SP signal (~50 mV).

Capasso et al. (2000) analysed partial pressures of He and CO_2 of some water samples from the north-eastern quarter of La Fossa cone area. They observed that the values of these partial pressures were appreciably higher than those in waters in equilibrium with the atmosphere, therefore showing interaction between volcanic gases and groundwater. Our data are consistent with those results and we interpret the gradient observed along Profile 4 as the evidence of preferential hot fluid circulations at the base of the north-western flank of La Fossa cone. The peaks of CO_2 flux in our data, around Palizzi are consistent with soil gas samples analysed by Capasso et al. (1997) in the same zone. The authors measured widespread exhalative manifestations dominated by CO_2 on Palizzi that they interpreted in terms of hydrothermal circulation. The local anomalies we observed and the associated vertical limit pointed out by the ERT data lead us to interpret this signal as hydrothermal fluid circulation rising along a volcano-tectonic structure. This structure could be related to the NNW Tindari-Letojanni regional fault system, identified in the southern sector of La Fossa caldera (Barberi et al., 1994). The northern boundary of the resistive body is not deeply rooted as is the southern one. This limit is likely only a lithological transition. The resistive rocks, probably a lava flow pile or a lava dome, constitute an impermeable limit to fluid circulation. The anomalies registered here are likely due to circulation of fluids guided along the lithological boundary.

4.5~~.3.~~ Comparison between the data and the geology ~~field observations~~

4.5.1. Signals associated to the various volcanic formations

The ERT data allow visualizing almost the entire cone above sea level. The profiles detailed in the following paragraphs cross the main structures identified on the volcanic edifice. In the first layers of the sections, the ERT data can be easily correlated to field observations. Indeed, in all the profiles, the Gran Cratere grey ash formation appears as a high-resistivity layer (see Figures 4, 5, 7, 8). At the base of this resistive layer, the sharp transition in electrical resistivity can be interpreted as a sharp lithological transition. Thereby this interface ~~first layer~~ can be followed at depth, along the slopes of the cone. The ERT sections display a thickness of ~20-30 m which could be attributed to the presence of the Gran Cratere, the Pietre Cotte and, the Forgia Vecchia formations.

The tuff outcrops, mostly corresponding to the Palizzi and Caruggi pyroclastic formations, are correlated to low resistivity values (< 20 Ω.m). This is visible in various outcrops as in the northern part of profile 6 (Fig. 7). These low resistivity values result from the cation exchange capacity of clay minerals and zeolites composing the Vulcano tuff and are indicative of the alteration of the rock (see Roberts and Lin, 1997; Revil et al., 2002; Bernard et al., 2007).

Also in the southern part of Profile 8, the GC crater cliff shows the ~~this~~ succession of an upper electrical resistive layer overlying a conductive layer (Fig. 8). In the field they are related respectively to (1) the Gran Cratere ash and Pietre Cotte deposits and (2) to the Caruggi tuff deposits (see the simplified geologic map of Figure 1).

4.5.2. Signals associated to the fumaroles

In the field, the fumaroles are concentrated along the most recent crater rims. The fumarolic fields inside the GC crater coincide with very low resistivity values, in the same order of magnitude than the tuffs deposits. The difference between “cold” tuffs and rocks affected by hydrothermal convection is highlighted by field observations, self-potential, temperature, and CO_2 flux measurements. Profile 6 shows highly conductive terrains (< 20 Ω.m) right under the most active fumaroles of La Fossa cone (Fig. 7). These conductive values are correlated with a temperature anomaly reaching 95°C, a positive self-potential anomaly of 100 mV (variation with respect to the mean SP value in this zone) and a CO_2 flux peak reaching ~10,000 g/m².d in the vicinity of the fumaroles. The most striking feature is the resistivity model showing a conductive channel running from the fumaroles at the surface, to the central hydrothermal system, until the maximum depth of investigation. The channel is progressively widening with depth. It developed thanks to a pre-existent structural limit, which is the GC crater.

4.5.3. Signals associated to crater boundaries

The craters identified through the morphology of the edifice and from a previous work (De Astis et al., 2007) are correlated with sharp horizontal transitions of resistivity forming more or less vertical limits. The best example is given by the south-west border of the GC crater which is crossed by profiles 1 and 8 (figures 4 and 8). It displays a vertical to slightly reverse-slope border delimiting high resistivities (> 150 Ω.m) outside the crater and low resistivities (< 20 Ω.m) inside the crater. ~~Moreover~~ As seen before, at the surface, a clear anomaly in temperature, self-potential, and CO_2 flux, spots this boundary, at the base of the crater cliff. This type of configuration, related to a structural limit, can be observed for most of the crater rims identified.

The reverse dip of the crater border faults is a common consequence of caldera-type or pit-crater-type collapse of a crater roof (e.g. Anderson, 1936; Branney, 1995; Acocella et al., 2000; Roche et al., 2000 and 2001; Walter and Troll, 2001). Therefore, GC crater could have been affected by this type of collapse during its formation. A similar dipping is not observed on the north-eastern border maybe because the collapse was asymmetric. Hydrothermal circulations and alteration in the vicinity of the eastern magma body evidenced under the PN crater could also have modified the resistivity distribution appearing nowadays and distort the observation on this side (Cf. next section: 4.6. The Eastern electrical resistive body).

4.6.~~4.~~ ~~Interpretation of~~ The eastern electrical resistive body

On all the sections crossing the eastern half of the edifice, a wide resistive body has been highlighted inside the PN crater, buried under younger formations. Profiles 1, 5, 6, 7, 8, and 9 (see Figure 2 for position of the profiles) clearly show a zone of resistivities ranging from 200 Ω.m to 1000 Ω.m, at depth. These high resistivity zones are in the range of the values expected for a lava flow pile or intrusive rocks (a dyke system, a shallow magma batch or a dome; e.g., see Figure 1.5 of Loke, 2004). The resistivity of the terrain depends mainly on the interconnected porosity of the rock and on the resistivity of the pore fluids. As an example, in a dome, a significant proportion of the vesicles are isolated and refilled by volcanic gas (e.g., see Ramsey and Fink, 1999) which confers a high resistivity to the rock.

It is important to notice that the inversion of ERT data tends to smooth the resistivity transitions i.e. the interfaces between the different geologic units. The boundary of the electrical resistive body is delimited by a sharp variation of the resistivity values, which can be associated to a lithological transition. On the resistivity models, the sharper transition is observed for an average value of ~160 Ω.m. Based on this assessment, the minimum depth of the resistive body can be estimated to ~50 m. This suggests that this unit is buried under additional formations than just the Gran Cratere pyroclastic deposits.

The density of the inverted resistivity data allowed us to reconstruct the shape of this resistive body buried inside the Punte Nere crater. To this purpose, the six ERT profiles cited above have been used. On each profile, the 160 Ω.m isoresistivity line has been digitized with one point every 20 m (in the horizontal plane). The XYZ coordinates obtained were interpolated and represented as a surface map (Fig. 9).

The lateral and vertical maximum extension of the body is not accessible as it extends under the depth of investigation. It displays a crescent shape with an irregular surface. The eastern side is a more or less regular slope, slightly steeper than the topographic surface while, to the West, the resistive body ends with a vertical boundary. This straight western limit coincides nicely with the PC crater rim.

Blanco-Montenegro et al. (2007) found a magnetic anomaly inside the PN crater. The authors interpreted this anomaly as a pile of tephritic lavas emplaced in an early phase of activity of La Fossa cone. From our ERT data, the shape, position and range of resistivity of this body led us to interpret it as an intrusion or a dome contemporary of the activity of the PN cone (5.3 ka – 3.8 ka) and truncated to the west, on at least 200 m depth by the PC crater ring fault during its formation (1739 A.D.) (See Figure 10). The presence of this large buried magma body, if it is not totally cooled down and degassed, can contribute to the thermal and CO_2 flux anomalies observed inside the PN crater (Fig. 8).

5. Conclusions

All the geophysical and geochemical anomalies we evidenced at the surface of La Fossa cone are controlled by structural limits. The main hydrothermal system is enclosed by the boundaries of the PC and GC craters. This is indicated by the low resistivity value of the formations and by the strong self-potential, CO_2 flux, and temperature anomalies measured in the limits of these craters. The hydrothermal activity is not restricted to the central part of the edifice. In the periphery, hydrothermal circulations have been evidenced and are, most of the time, clearly influenced by the structure of the edifice. This structure corresponds either to lithological levels or to structural limits and the following conclusions have been reached:

(1) The hydrothermal fluids rising from the central hydrothermal system of the GC crater condensate at shallow depth and partly flow down to the PN crater, through the more permeable levels. They are guided along the PC crater border and the resistive body highlighted at depth by ~~the~~ electrical resistivity tomography.

(2) The Palizzi area is affected by circulations of hydrothermal fluids associated to the presence of a vertical structural limit visible in the resistivity tomography at the base of the edifice. This fault reaching more than 100 m b.s.l. could be attributed to the NNW regional volcano-tectonic orientation affecting the island of Vulcano.

(3) The former-crater rims, even when partially buried, remain preferential paths for hydrothermal fluid circulations as evidenced for the FV, PN, and Pa craters, which are underlined by strong temperature and CO_2 degassing anomalies and associated with low resistivity values at depth.

Circulations of hydrothermal fluids have been evidenced at the base of the north-western flank, by a variation ~~gradient~~ of temperature of ~6°C from the south-east to the north-west along the profile 4. Such a distal anomaly of temperature can be due either to rising hydrothermal fluids or to fluids contaminated by the hydrothermal release in the summit area and flowing down to the base into shallow ground levels of the north-western flank. The north-western end of Profile 4 could be a relevant site for monitoring the temperature variations, if the fluctuations of the main hydrothermal system activity influence also the hydrothermal circulations at the base of the cone.

Our study also reveals the presence of an old magmatic body, dome or shallow intrusion, associated to the activity of the Punte Nere cone. The PC crater intersects this magma body on 200 m high, destructing its western part during the formation of the crater. The interface between the resistive body and the deposits filling the inner crater is one of the major structural limits of the edifice and constitute the eastern limit of the main hydrothermal system of La Fossa cone.

Acknowledgments. We thank Xavier Rassion for his help in the field. A special thanks to Maria Marsella for providing us the high resolution orthophoto and the digital elevation model of Vulcano Island. The INSU-CNRS, Istituto di Metodologie per l'Analisi Ambientale (IMAA) del CNR, the Laboratoire GéoSciences Réunion-IPGP, the CNR, the Istituto Nazionale di Geofisica e Vulcanologia (INGV), and the Dipartimento per la Protezione Civile through the DPC Projects (Sub-project V3.5 Vulcano, Agreement 2005-2007) are thanked for financial supports. We also thank Andrea Borgia for interesting discussions. This is IPGP contribution number: 2446. We thank the editor, Joan Marti, an anonymous referee, and Jean-François Lénat for their very useful comments on our manuscript.

References

Acocella, V., Cifelli, F., Funiciello, R., 2000. Analogue models of calderas and resurgent domes. J. Volcanol. Geotherm. Res. 104, 81-96.

Allard, P., Carbonnelle, J., Dajlevic, D., Le Bronec, J., Morel, P., Robe, M. C., Morenas, J.M., Faivre-Pierret, R., Martin, D., Sabroux, J.C., Zettwoog, P., 1991. Eruptive and diffuse emissions of CO_2 from Mount Etna. Nature 351, 387–391.

Anderson, E.M., 1936. The dynamics of the formation of cone sheets, ring dikes, and cauldron subsidences. Proceedings of the Royal Society of Edinburgh 56, 128–163.

Arrighi, S, Tanguy, J.-C., Rosi, M., 2006. Eruptions of the last 2200 years at Vulcano and Vulcanello (Aeolian Islands, Italy) dated by high accuracy archeomagnetism. Phys. Earth Planet. Int. 159, 225–233. doi:10.1016/j.pepi.2006.07.010

~~Aubert, M., Kieffer, G., 1984. Evolution d'une intrusion magmatique dans le flanc sud de l'Etna entre juin 1982 et juin 1983. Résultats de potentiel spontané (PS) et essai d'interprétation de l'éruption de 1983. C. R. Acad. Sci. Paris t.296 (Série II-8), 379-382.~~

Aubert, M., Lima, E., 1986. Hydrothermal activity detected by self-potential measurements (SP) at the N-S volcanic axis between the volcanoes "Nevado de Colima" and "Fuego de Colima", Mexico. Geophys. J. Int., 25-4: 575-586.

Aubert, M., Baubron, J.-C., 1988. Identification of a hidden thermal fissure in volcanic terrain, using a combination of hydrothermal convection indicators and soil-atmosphere analysis. J. Volcanol. Geotherm. Res. 35, 217-225.

Aubert, M., Diliberto, S., Finizola, A., Chébli, Y., 2007. Double origin of hydrothermal convective flux variations in the Fossa of Vulcano (Italy). Bull. Volc. doi 10.1007/s00445-007-0165-y

Auken, E., Christiansen, A. V., 2004. Layered and laterally constrained 2D inversion of resistivity data. Geophysics, 69, 752–761.

Barberi, F., Neri, G., Valenza, M., Villari, L., 1991. 1987–1990 unrest at Vulcano. Acta Vulcanol. 1, 95–106.

Barberi, F., Gandino, A., Gioncada, A., La Torre, P., Sbrana, A., Zenucchini, C., 1994. The deep structure of the Eolian Arc (Filicudi-Panarea-Vulcano sector) in light of gravimetric, magnetic and volcanological data. J. Volcanol. Geotherm. Res. 61, 189-206.

Baubron, J.C., Allard, P., Toutain, J.P., 1990. Diffuse volcanic emissions of carbon dioxyde from Vulcano Island, Italy. Nature 344, 51-53.

Bernard, M.-L., Zamora, M., Géraud, Y., Boudon, G., 2007. Transport properties of pyroclastic rocks from Montagne Pelée volcano (Martinique, Lesser Antilles). J. Geophys. Res. 112, B05205, doi:10.1029/2006JB004385.

Binley, A., Kemna, A., 2005. DC resistivity and induced polarization methods. In Hydrogeophysics, edited by Y. Rubin and S. Hubbard, chap. 5, pp. 129– 156, Springer, New York.

Blanco-Montenegro, I., de Ritis, R., Chiappini, M., 2007. Imaging and modelling the subsurface structure of volcanic calderas with high-resolution aeromagnetic data at Vulcano (Aeolian Islands, Italy). Bull. Volc. 69, 643-659. doi 10.1007/s00445-006-0100-7

Branney, M.J., 1995. Downsag and extension at calderas: new perspectives on collapse geometries from ice-melt, mining, and volcanic subsidence. Bull. Volcanol. 57, 303– 318.

Bukumirovic, T., Italiano, F., Nuccio, P.M., 1997. The evolution of a dynamic geological system: the support of a GIS for geochemical measurements at the fumarole field of Vulcano, Italy. J. Volcanol. Geotherm. Res. 79, 253-263.

Capasso, G., Favara, R., Inguaggiato, S., 1997. Chemical features and isotopic composition of gaseous manifestations on Vulcano Island, Aeolian Islands, Italy: An interpretative model of fluid circulation. Geochimica et Cosmochimica Acta vol. 61, No. 16, 3425-3440.

Capasso, G., Favara, R., Inguaggiato, S., 2000. Interaction between fumarolic gases and thermal groundwaters at Vulcano Island (Italy): evidences from chemical composition of dissolved gases in waters. J. Volcanol. Res. 102, 309-318.

Cecchi, E., Van Wyk de Vries, B., Lavest, J.-M., 2005. Flank spreading and collapse of weak-cored volcanoes. Bull. Volcanol. 67, 72–91.

Chébli, Y., 1997. Tomographie thermique et géoélectrique du cratère du Vulcano. Mémoire de D.E.A. Processus Magmatiques et Métamorphiques - Volcanologie, Université Blaise Pascal, Clermont-Ferrand II, 60 pp.

Chiodini, G., Cioni, R., Guidi, M., Marini, L., Raco, B., 1998. Soil CO_2 flux measurements in volcanic and geothermal areas. Appl. Geochem. 13, 543-552.

Day, S. J., 1996. Hydrothermal pore fluid pressure and the stability of porous, permeable volcano. In Volcano Instability o the Earth and Other Planets, McGuire W. J., Jones A. P., and Neuberg J. (Eds), Geol. Soc. Spec. Publ. 110, 77-93.

De Astis, G., Frazzetta, G., La Volpe, L., 1989. I depositi di riempimento della Caldera del Piano e i depositi della Lentia. Boll. G.N.V. 1989 (2), 763-778.

De Astis, G., La Volpe, L., Peccerillo, A., Civetta, L., 1997. Volcanological and petrological evolution of Vulcano island (Aeolian Arc, southern Tyrrhenian Sea). J. Geophys. Res. 102, B4, 8021–8050.

De Astis, G., Ventura, G., Vilardo, G., 2003. Geodynamic significance of the Aeolian volcanism (Southern Tyrrhenian Sea, Italy) in light of structural, seismological, and geochemical data. Tectonics 22, 4, 14.1–14.17.

De Astis, G., Dellino, P., La Volpe, L., Lucchi, F., Tranne, C.A., 2007. Geological map of the Vulcano Island, 1:10000, L. La Volpe & G. De Astis Eds.

Dellino, P, La Volpe, L., 1997. Stratigrafia, dinamiche eruttive e deposizionali, scenario eruttivo e valutazioni di pericolosità a La Fossa di vulcano. In : “CNR-GNV Progetto Vulcano 1993-1995” L. La Volpe, P. Dellino, M. Nuccio, E. Privitera, and A. Sbrana (Ed), Felici, Pisa, 214-237.

De Rosa, R., Calanchi, N., Dellino, P.F., Francalanci, L., Lucchi, F., Rosi, M., Rossi, P.L., Tranne, C.A., 2004. 32nd International Geological Congress, Field Trip Guide Book – P42, vol. n°5: Geology and volcanism of Stromboli, Lipari, and Vulcano (Aeolian Islands); Firenze 20-28 agosto 2004.

Durand, S., 1997. Etude structurale de la zone sommitale du Karthala (Grande Comore) par polarisation spontanée. Travail d'Etude et de Recherche. Univ. Blaise Pascal, Clermont-Ferrand II, 26 pp.

Finizola, A., Sortino, F., Lénat, J.-F., Valenza, M., 2002. Fluid circulation at Stromboli volcano (Aeolian Islands, Italy) from self potential and CO_2 surveys. J. Volcanol. Geotherm. Res. 116, 1-18.

Finizola, A., Sortino, F., Lénat, J-F., Aubert, M., Ripepe, M., Valenza, M., 2003. The summit hydrothermal system of Stromboli: New insights from self-potential, temperature, CO_2 and fumarolic fluids measurements, with structural and monitoring implications. Bull. Volcanol. 65, 486-504. doi:10.1007/s00445-003-0276-2

Finizola, A., Lénat, J.-F., Macedo, O., Ramos, D., Thouret, J.-C., Sortino, F., 2004. Fluid circulation and structural discontinuities inside Misti volcano (Peru) inferred from self-potential measurements. J. Volcanol. Geotherm. Res. 135, 343-360.

Finizola, A., Revil, A., Rizzo, E., Piscitelli, S., Ricci, T., Morin, J., Angeletti, B., Mocochain, L., Sortino, F., 2006. Hydrogeological insights at Stromboli volcano (Italy) from geoelectrical, temperature, and CO_2 soil degassing investigations. Geophys. Res. Lett. 33, L17304. doi: 10.1029/2006GL026842.

Frazzetta, G., La Volpe, L., Sheridan, M.F., 1983. Evolution of the Fossa cone, Vulcano. J. Volcanol. Geotherm. Res. 17, 329–360.

Frazzetta, G., Gillot, P.Y., La Volpe, L., Sheridan, M.F., 1984. Volcanic hazards at Fossa of Vulcano: data from the last 6000 years. Bull. Volcanol. 47, 105–124.

Ghisetti, F., 1979. Relazioni tra strutture e fasi trascorrenti e distensive lungo i sistemi Messina-Fiumefreddo, Tindari-Letojanni e Alia-Malvagna (Sicilia nord-orientale): uno studio microtettonico. Geol. Rom. 18, 23-56.

Granieri, D., Carapezza, M.L., Chiodini, G., Avino, R., Caliro, S., Ranaldi, M., Ricci, T., Tarchini, L., 2006. Correlated increase in CO_2 fumarolic content and diffuse emission from la Fossa crater (Vulcano, Italy): Evidence of volcanic unrest or increasing gas release from a stationary deep magma body ? Geophys. Res. Lett. 33, L13316. doi:10.1029/2006GL026460.

Griffiths, D.H., Barker, R.D., 1993. Two-dimensional resistivity imaging and modelling in areas of complex geology. J. Appl. Geophys. 29, 211-226.

Ishido, T., 2004. Electrokinetic mechanism for the "W"-shaped self-potential profile on volcanoes. Geophys. Res. Lett. 31, L15616, doi:10.1029/2004GL020409.

~~Jardani, A., Revil, A., Bolève, A., Dupont, J. P., Barrash, W., Malama, B., 2007. Tomography of groundwater flow from self-potential (SP) data. Geophysical Research Letters 34, L24403. doi:10.1029/2007GL031907.~~

~~Jardani, A., Revil, A., Bolève, A., Dupont, J. P., 2008. Three-dimensional inversion of self-potential data used to constrain the pattern of ground water flow in geothermal fields. J. Geophys. Res. 113. doi:10.1029/2007JB005302.~~

Keller, J., 1970. Die historischen eruptionen von Vulcano und Lipari, Zeit. Deut. Geol. Ges. 121, 179–185.

Keller, J., 1980. The island of Vulcano. Rend. Soc. Ital. Mineral. Petrol. 36, 369-414.

Lénat, J.F., Robineau, B., Durand, S., Bachèlery, P., 1998. Etude de la zone sommitale du volcan Karthala (Grande Comore) par polarisation spontanée. C. R. Acad. Sci. 327, 781–788.

Lo Cascio, P., Navarra, E., 1997. Guida Naturalistica Alle Isole Eolie. L'EPOS, Palermo. 112p.

Loke, M.H., 2004. Tutorial 2-D and 3-D electrical imaging surveys. Geotomo Software, Malaysia, 128p.

Loke, M.H., Barker, R.D., 1996. Rapid least-square inversion of apparent resistivity pseudosections by a quasi-Newton method. Geophys. Prospect. 44, 131-152.

López, D. L., Williams, S. N., 1993. Catastrophic volcanic collapse: relation to hydrothermal processes. Science 260, 1794-1796.

Malengreau, B., Lénat, J.-F., Bonneville, A., 1994. Cartographie et surveillance temporelle des anomalies de polarisation spontanee (PS) sur le Piton de la Fournaise: Cartography and temporal observation of self-potential (SP) anomalies at Piton de la Fournaise. Bull. Soc. Geol. Fr. 165(3), 221–232.

Mazzuoli, R., Tortorici, L., Ventura, G., 1995. Oblique rifting in Salina, Lipari and Vulcano islands (Aeolian islands, southern Italy). Terra Nova 7, 444-452.

Merle, O., Lénat, J.-F., 2003. Hybrid collapse mechanism at Piton de la Fournaise volcano, Reunion Island, Indian Ocean. J. Geophys. Res. 108, B3, 2166.

Michel, S., Zlotnicki, J., 1998. Self-potential and magnetic surveying of La Fournaise Volcano (Reunion Island): Correlations with faulting, fluid circulation, and eruption. J. Geophys. Res. 103, 17,845–17,857.

Montalto, A., 1994. Seismic signals in geothermal areas of active volcanism: a case study from “La Fossa”, Vulcano (Italy). Bull. Volcanol. 56, 220–227.

Pribnow, D. F. C., Schütze, C., Hurter, S. J., Flechsig, C., Sass, J. H., 2003. Fluid flow in the resurgent dome of Long Valley Caldera: implications from thermal data and deep electrical sounding. J Volcanol Geotherm Res 127, 329-345

Rabaute, A., Revil, A., Brosse E., 2003. In situ mineralogy and permeability logs from downhole measurements. Application to a case study in clay-coated sandstone formations, J. Geophys. Res. 108, 2414. doi: 10.1029/2002JB002178.

Ramsey, M. S., Fink, J. H., 1999. Estimating silicic lava vesicularity with thermal remote sensing: a new technique for volcanic mapping and monitoring. Bull. Volc. 61, 32-39.

Reid, M. E., Sisson, T. W., Brien, D.L., 2001. Volcano collapse promoted by hydrothermal alteration and edifice shape, Mount Rainier, Washington. Geology 29, n° 9, 779-782.

Revil, A., Hermitte, D., Spangenberg, E., Cochémé, J. J., 2002. Electrical properties of zeolitized volcaniclastic materials. J. Geophys. Res. 107(B8), 2168. doi:10.1029/2001JB000599.

Revil, A., Finizola, A., Sortino, F., Ripepe, M., 2004. Geophysical investigations at Stromboli volcano, Italy: implications for ground water flow and paroxysmal activity. Geophys. J. Intern. 157, 426-440.

Revil, A., Finizola, A., Piscitelli, S., Rizzo, E., Ricci, T., Crespy, A., Angeletti, B., Balasco, M., Barde Cabusson, S., Bennati, L., Bolève, A., Byrdina, S., Carzaniga, N., Di Gangi, F., Morin, J., Perrone, A., Rossi, M., Roulleau, E., Suski, B., 2008. Inner structure of La

Fossa di Vulcano (Vulcano Island, southern Tyrrhenian Sea, Italy) revealed by high-resolution electric resistivity tomography coupled with self-potential, temperature, and CO_2 diffuse degassing measurements. J. Geophys. Res. 113, B07207. doi:10.1029/2007JB005394.

Ricci, T., 2007. Studio del degassamento diffuso di CO_2 e indagini geofisiche a finalità idrogeologica nei vulcani attivi di Stromboli e de La Fossa di Vulcano: variazioni temporali e loro significato vulcanologico, implicazioni strutturali, per il monitoraggio geochimico e per la pericolosità da gas. Phd Thesis, Università di Roma Tre

Roberts, J. J., Lin, W., 1997. Electrical properties of partially saturated Topopah Spring tuff: Water distribution as a function of saturation, Water Resour. Res., 33, 577– 587.

Roche O., Druit T.H., Merle, O., 2000. Experimental study of caldera formation. J. Geophys. Res. 105, N°B1, 395-416

Roche, O., van Wyk de Vries, B., Druitt, T.H., 2001. Sub-surface structures and collapse mechanisms of summit pit craters. J. Volcanol. Geotherm. Res. 105, 1-18

~~Straface, S., Falico, C., Troisi, S., Rizzo, E., Revil, A., 2007. An inverse procedure to estimate transmissivities from heads and SP signals. Ground Water 45(4), 420-428.~~

Vallance, J. W., Scott, K. M., 1997. The Osceola Mudflow from Mont Rainier: Sedimentology and hazard implications of a huge clay-rich debris flow. GSA Bulletin 109, n° 2, 143–163.

Van Wyk de Vries, B., Kerle, N., Petley, D., 2000. Sector collapse forming at Casita volcano, Nicaragua. Geology 28, n° 2, 167-170.

Ventura, G., 1994. Tectonics, structural evolution and caldera formation on Vulcano Island (Aeolian Archipelago, southern Tyrrhenian Sea). J. Volcanol. Geotherm. Res. 60, 207-224.

Ventura, G., Vilardo, G., Milano, G., Pino, N. A., 1999. Relationships among crustal structure, volcanism and strike-slip tectonics in the Lipari-Vulcano Volcanic Complex (Aeolian Islands, Southern Tyrrhenian Sea, Italy). Phys. Earth Planet Int., Volume 116, Issue 1-4, 31-52.

Voight, B., Elsworth, D., 1997. Failure of volcano slope. Géotechnique 47(1), 1-31.

Walter, T.R., Troll, V.R., 2001. Formation of caldera periphery faults: an experimental study. Bull. Volc. 63, 191-203.

Wohletz, K., Heiken, G., 1992. Volcanology and geothermal energy. J.H. Heiken (Ed.), University of California Press., 432p.

Zablocki, C.J., 1976. Mapping thermal anomalies on an active volcano by the self-potential method, Kilauea, Hawaii. Proceedings, 2nd U.N. Symposium on the development and use of geothermal resources, San Francisco, California, May 1975, 2, 1299-1309.

Figure captions:

Figure 1. Location of the studied area. Simplified geological map of La Fossa cone draped on the DEM (map simplified from de Astis et al., 2007) and chronology. PN (Punte Nere), Pa (Palizzi), FV (Forgia Vecchia), PC (Pietre Cotte), and GC (Gran Cratere) crater rims are represented. In the upper right corner, Vu, VP, and LFc stand for Vulcanello, Vulcano Primordiale and La Fossa cone. On the location and structural sketch map of the Aeolian Islands area M, AI, TL, and ME stand for the Marsili Oceanic Basin, the Aeolian Islands represented by white ellipses (red star for Vulcano; black shapes for seamounts), the Tindari-Letojanni fault system, and the Malta Escarpment fault system (sketch simplified from Ventura et al., 1999).

Figure 2. Location of the 9 profiles performed, on the orthophotography overlaid on the DEM of La Fossa cone. Bright orange profiles are those detailed in the text. White dots represent the measure points. The light pink areas on the flanks of the volcano correspond to the hydromagmatic tuff discussed in the main text.

Figure 3. Temperature, Self potential, and soil CO_2 flux maps of La Fossa cone, interpolated from the data of the nine profiles performed, overlaid on the DEM. White and black dots represent the measure points. PN (Punte Nere), Pa (Palizzi), FV (Forgia Vecchia), PC (Pietre Cotte), and GC (Gran Cratere) craters are localised with white dashed lines.

Figure 4. Temperature, self-potential, soil CO_2 flux, and electric resistivity tomography along Profile 1. Note the sharp resistivity transition on the GC crater boundaries. PN: Punte Nere crater, PC: Pietre Cotte crater, GC: Gran Cratere crater.

Figure 5. Temperature, self-potential, soil CO_2 flux, and electric resistivity tomography along profile 4. Note the sharp resistivity transition (black arrow) at a distance of 2000 m underlined by a temperature and soil CO_2 flux maximum. The black arrow is also localized on map in Figure 6.

Figure 6. Map representation of the temperature variation ~~gradient~~ at the base of the cone, along profile 4. White dots represent the measure points. The black arrow is pointing the resistivity transition highlighted by electrical resistivity tomography (see figure 5).

Figure 7. Temperature, self-potential, soil CO_2 flux, and electric resistivity tomography along profile 6. Note the correspondence of the temperature, self-potential, and soil CO_2 flux anomalies with low values of resistivities reaching the surface. PN: Punte Nere crater, PC: Pietre Cotte crater, GC: Gran Cratere crater, F: fumaroles.

Figure 8. Temperature, self-potential, soil CO_2 flux, and electric resistivity tomography along profile 8. Note the presence of a large resistive body under the Punte Nere former cone (see also profile 1 on figure 4). PN: Punte Nere crater, PC: Pietre Cotte crater, GC: Gran Cratere crater.

Figure 9. a. Image map of the electrical resistive body draped on the DEM; b. 3D view of the resistive body under a truncated DEM of La Fossa; c. 3D view of the resistive body from the south-east. The colour scale represents the elevation of the surface of the resistive body. Only the measured points used to build the 3D representation of the resistive body are visible (black and white dots). PN: Punte Nere, Pa: Palizzi, FV: Forgia Vecchia, PC: Pietre Cotte, and GC: Gran Cratere. Coordinates are in meter, UTM (WGS84).

Figure 10. Schematic representation of the evolution of the cone, from Punte Nere to nowadays. The information on both the geology and on the fluid circulation is shown. The synthetic sketch is based on Profile 8. PN: Punte Nere crater, PC: Pietre Cotte crater, GC: Gran Cratere crater.

Figure 1

Click here to download high resolution image

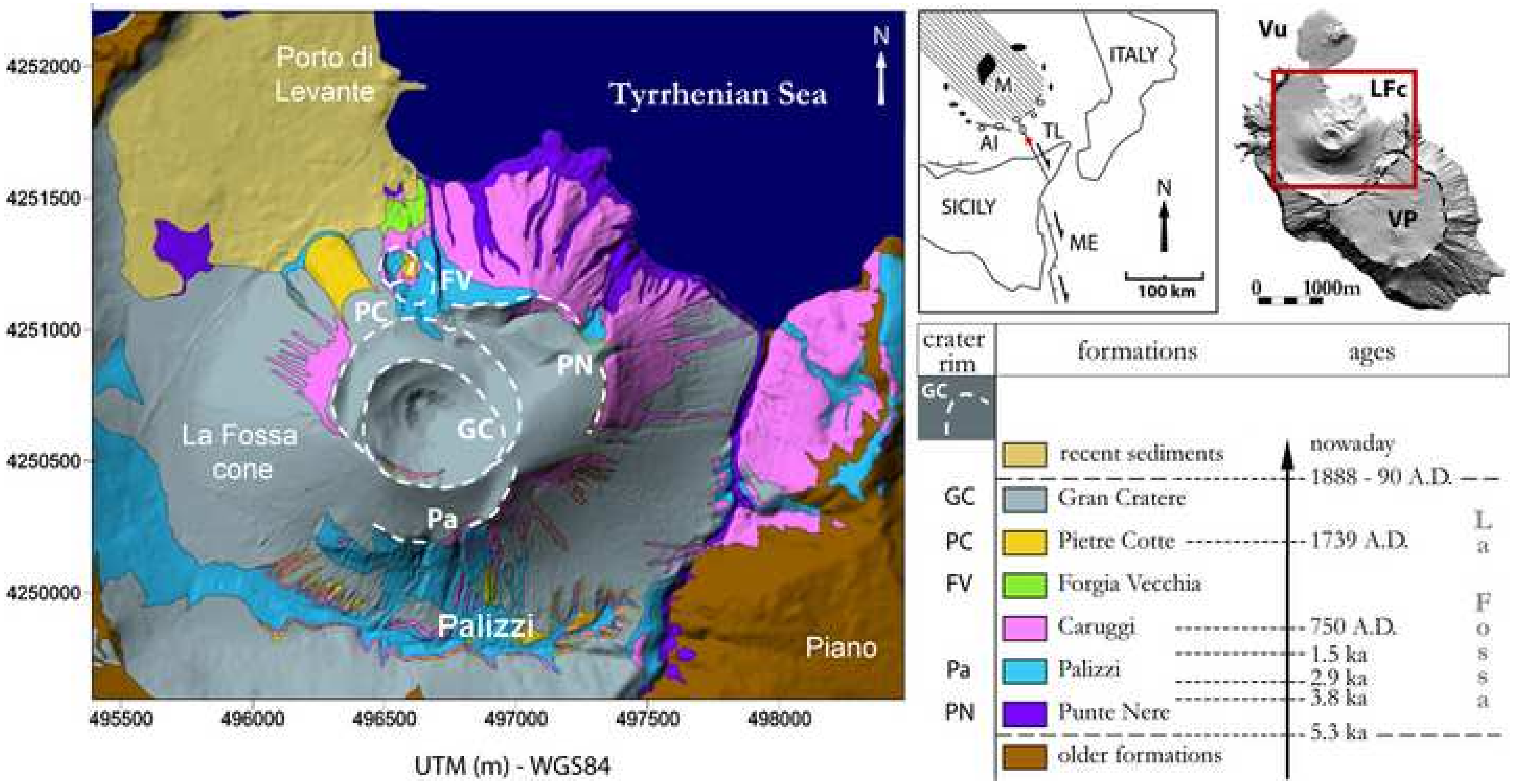

Figure 2
Click here to download high resolution image

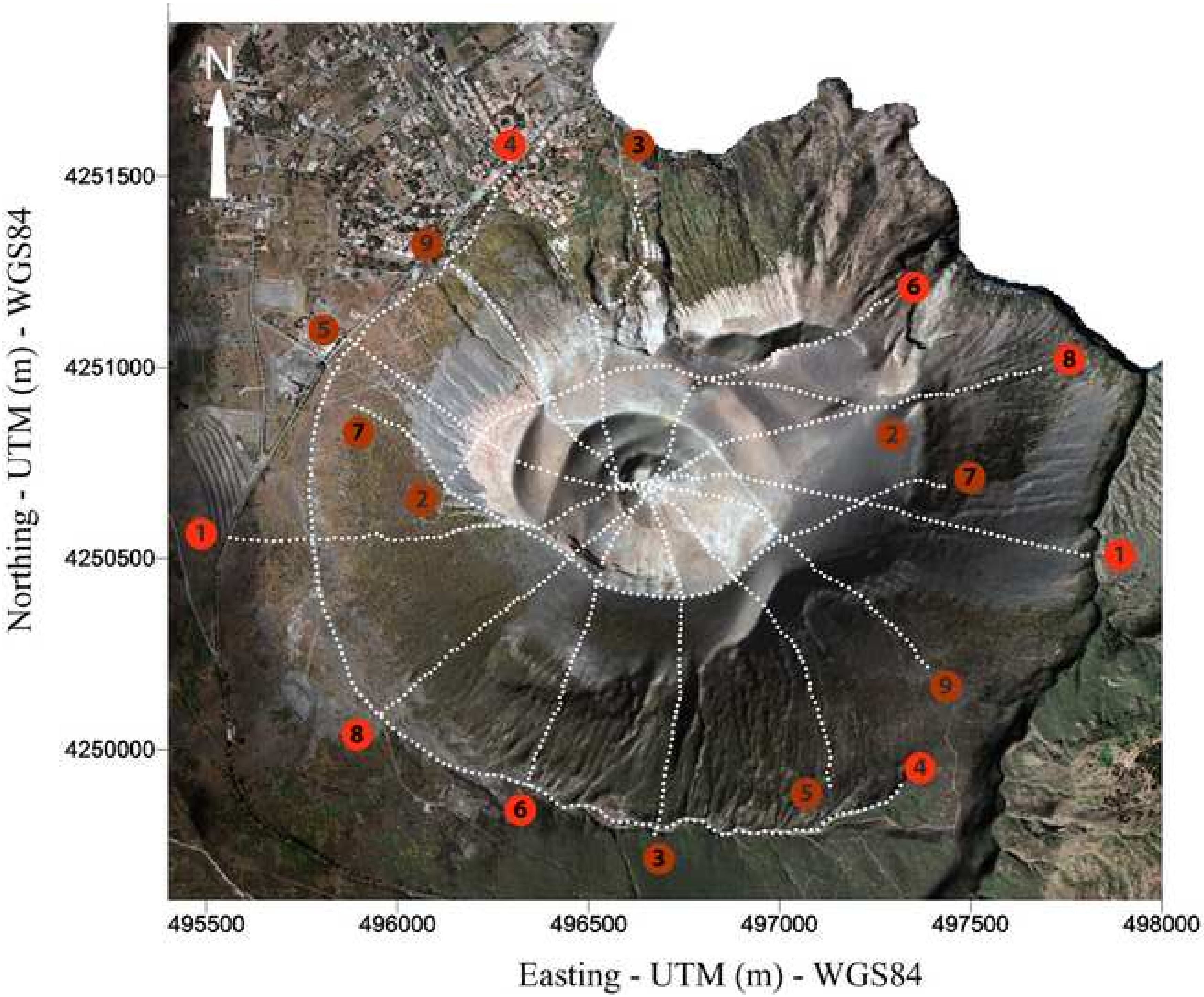

Figure 3

Click here to download high resolution image

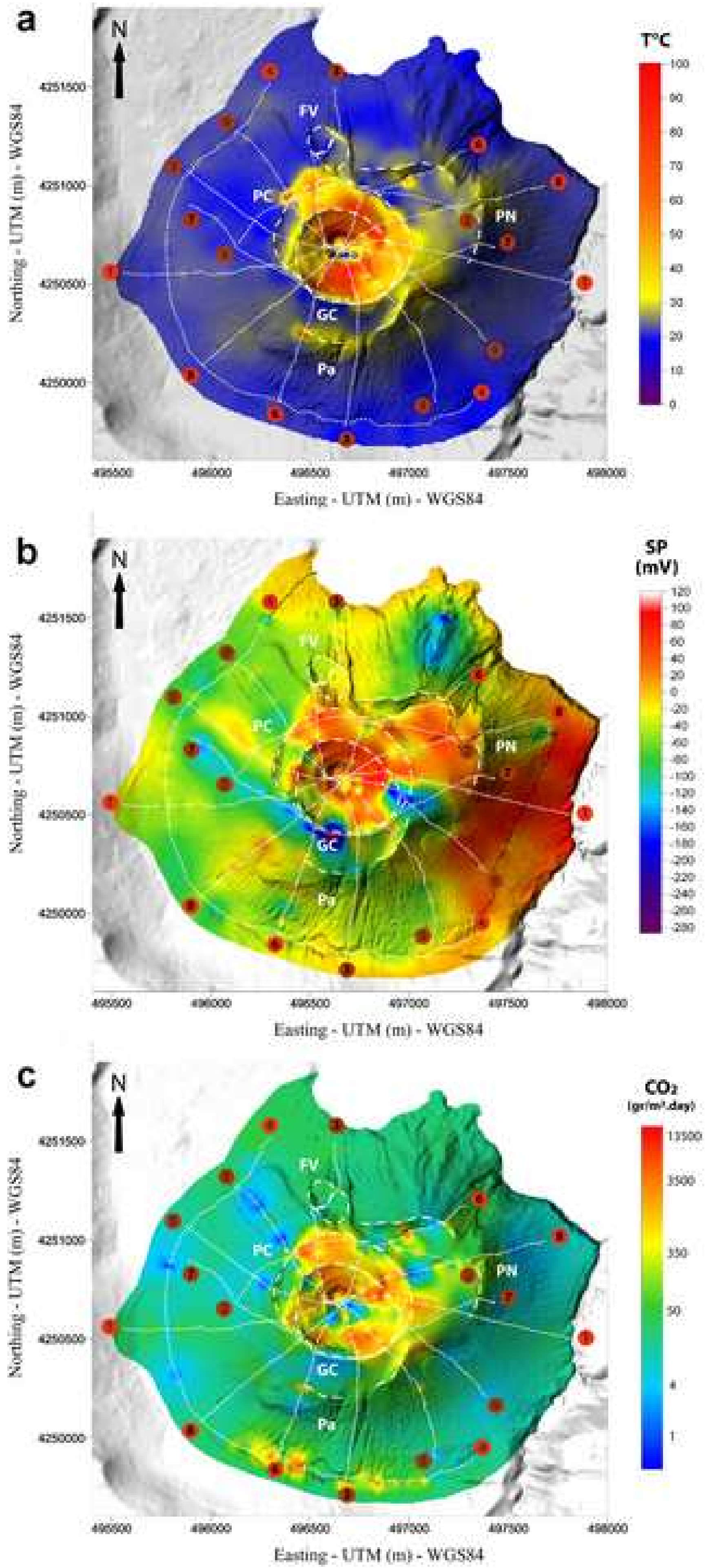

Figure 4
Click here to download high resolution image

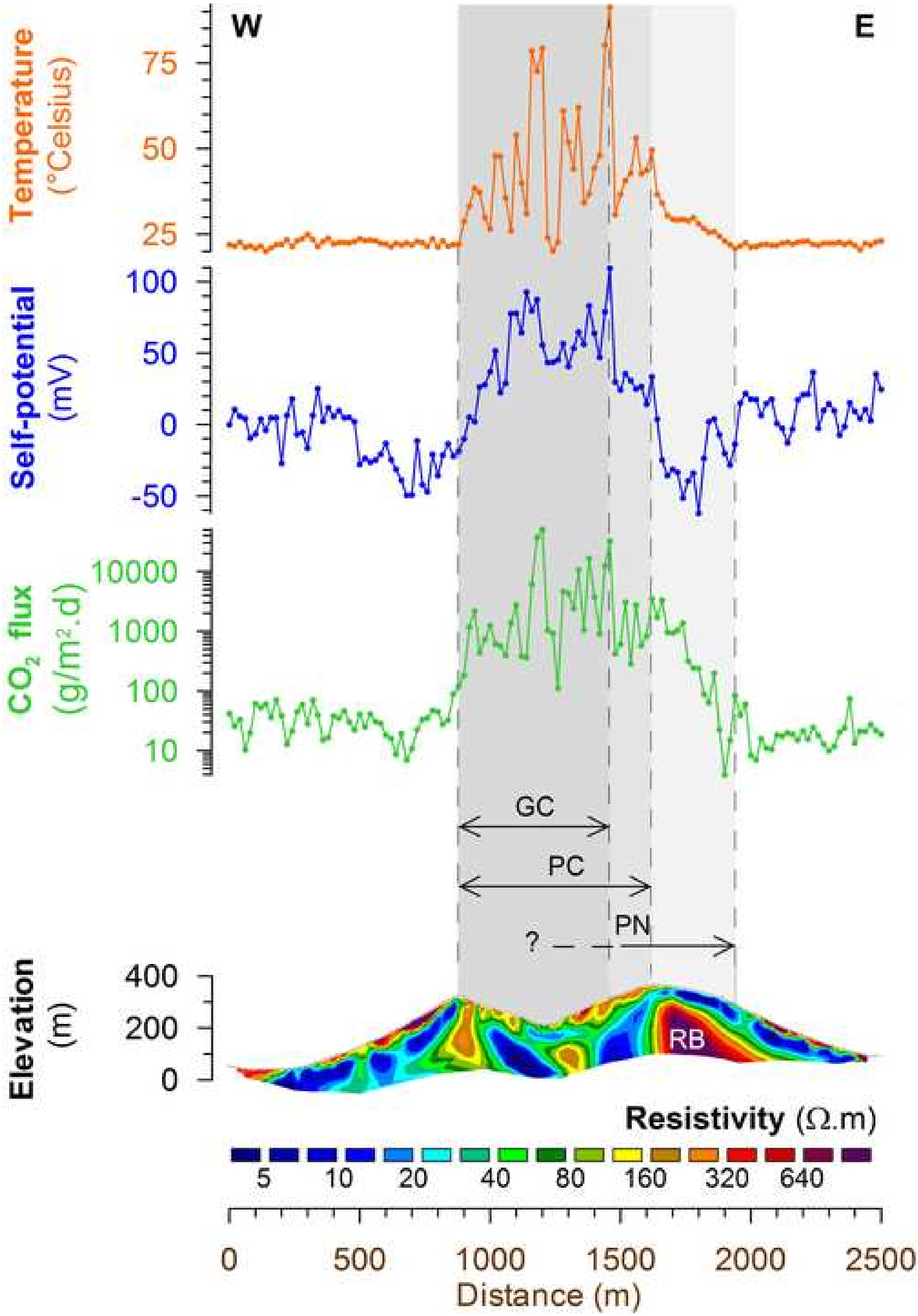

Figure 5
Click here to download high resolution image

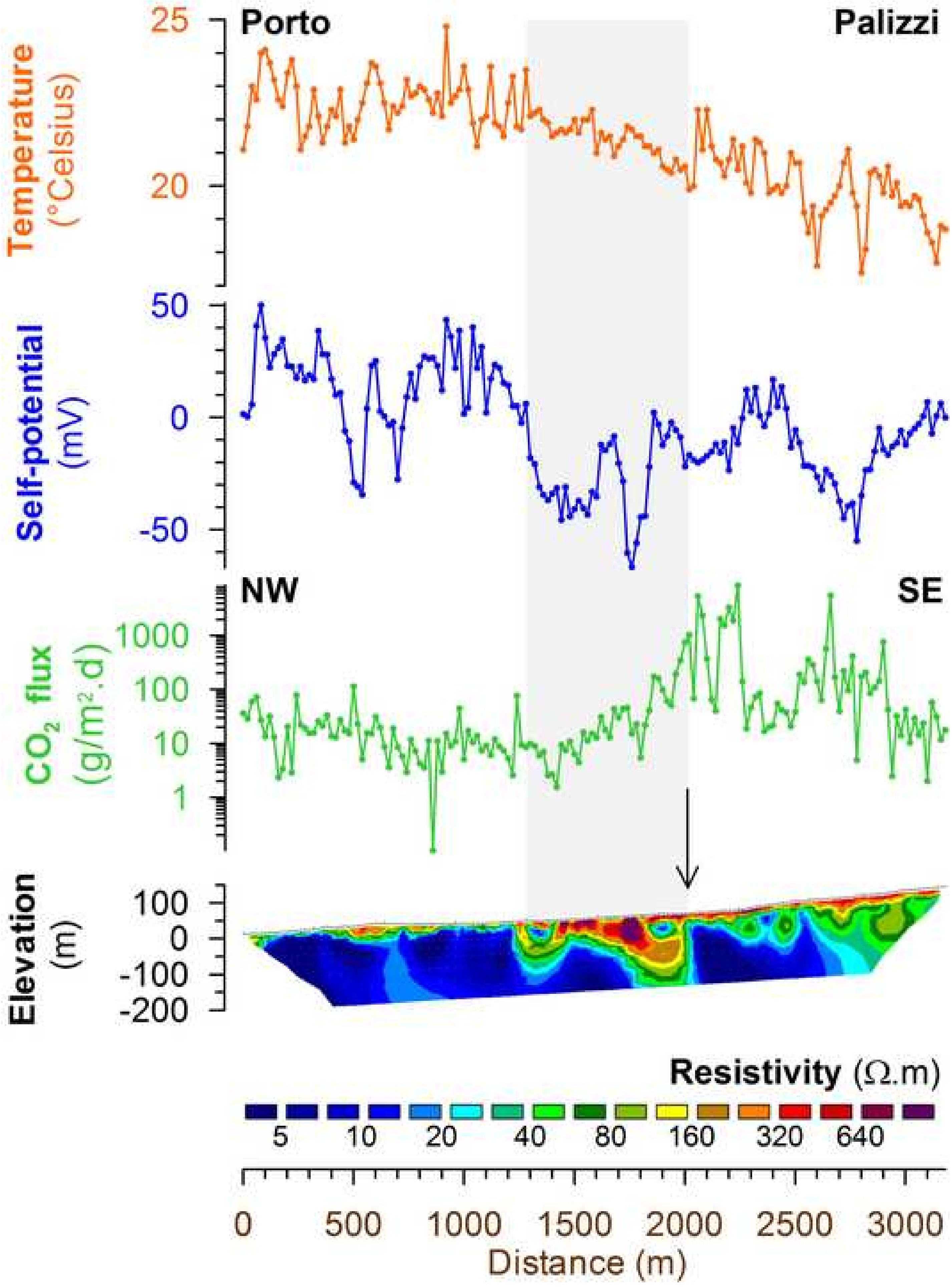

Figure 6
Click here to download high resolution image

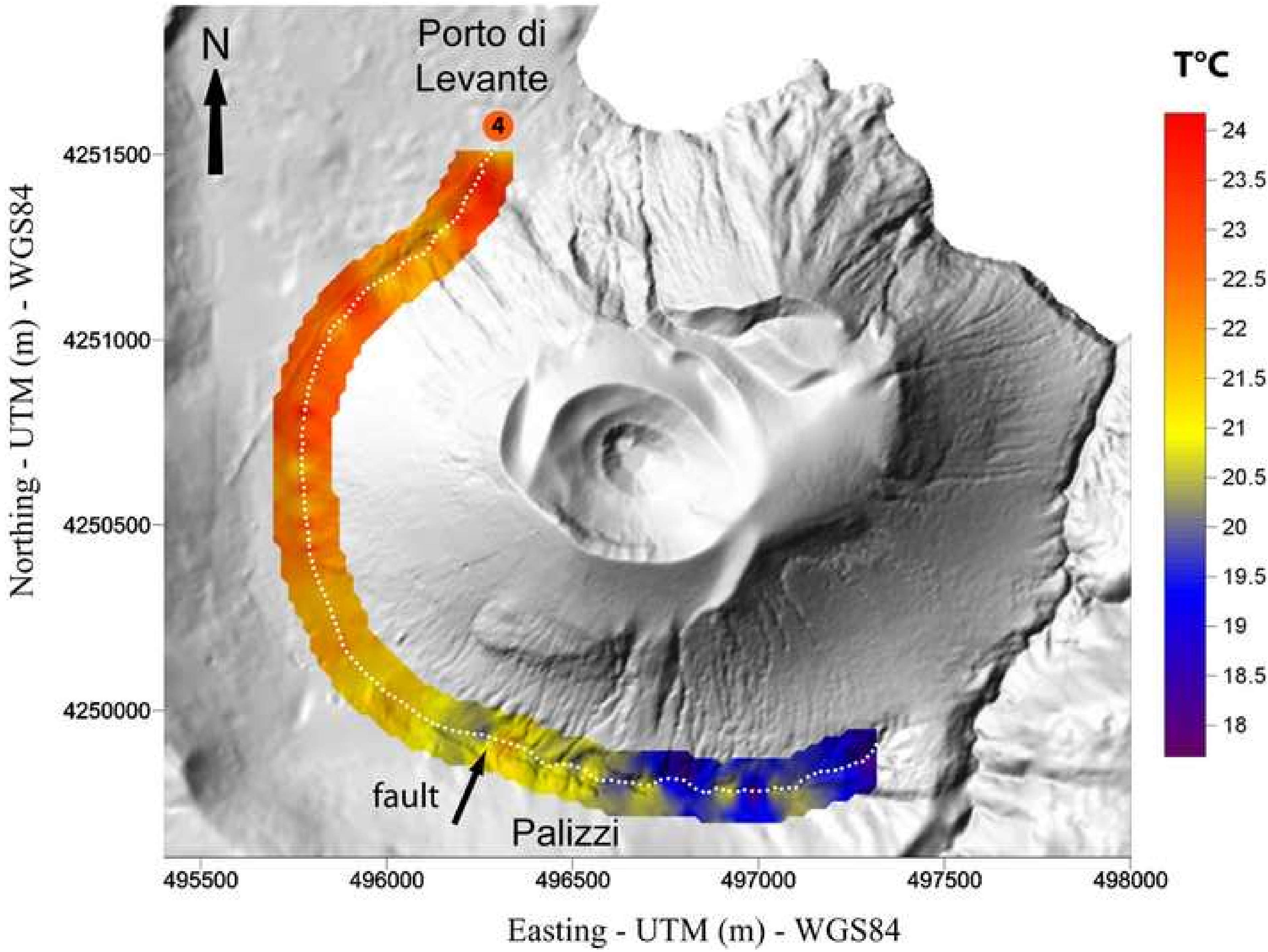

Figure 7
Click here to download high resolution image

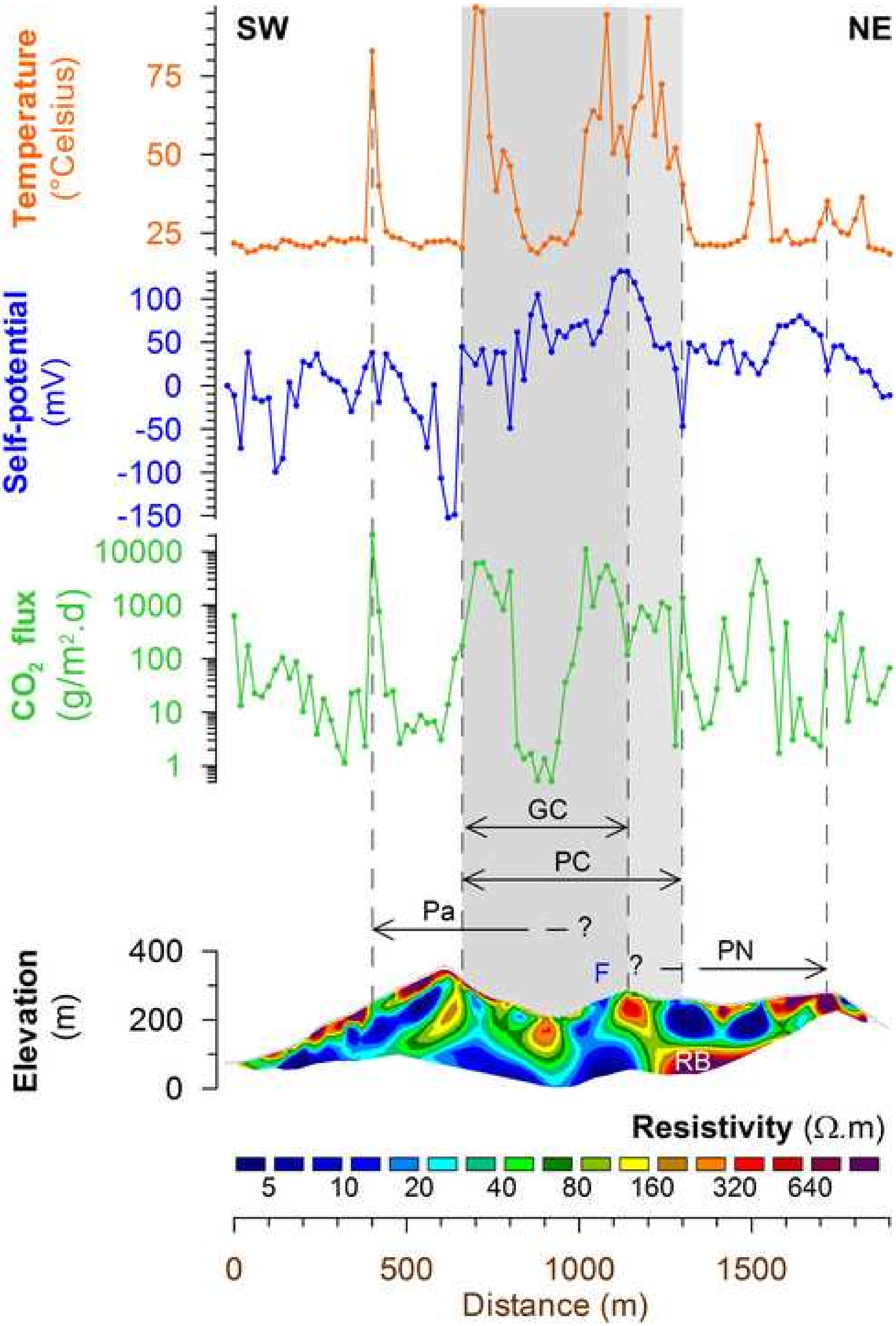

Figure 8
Click here to download high resolution image

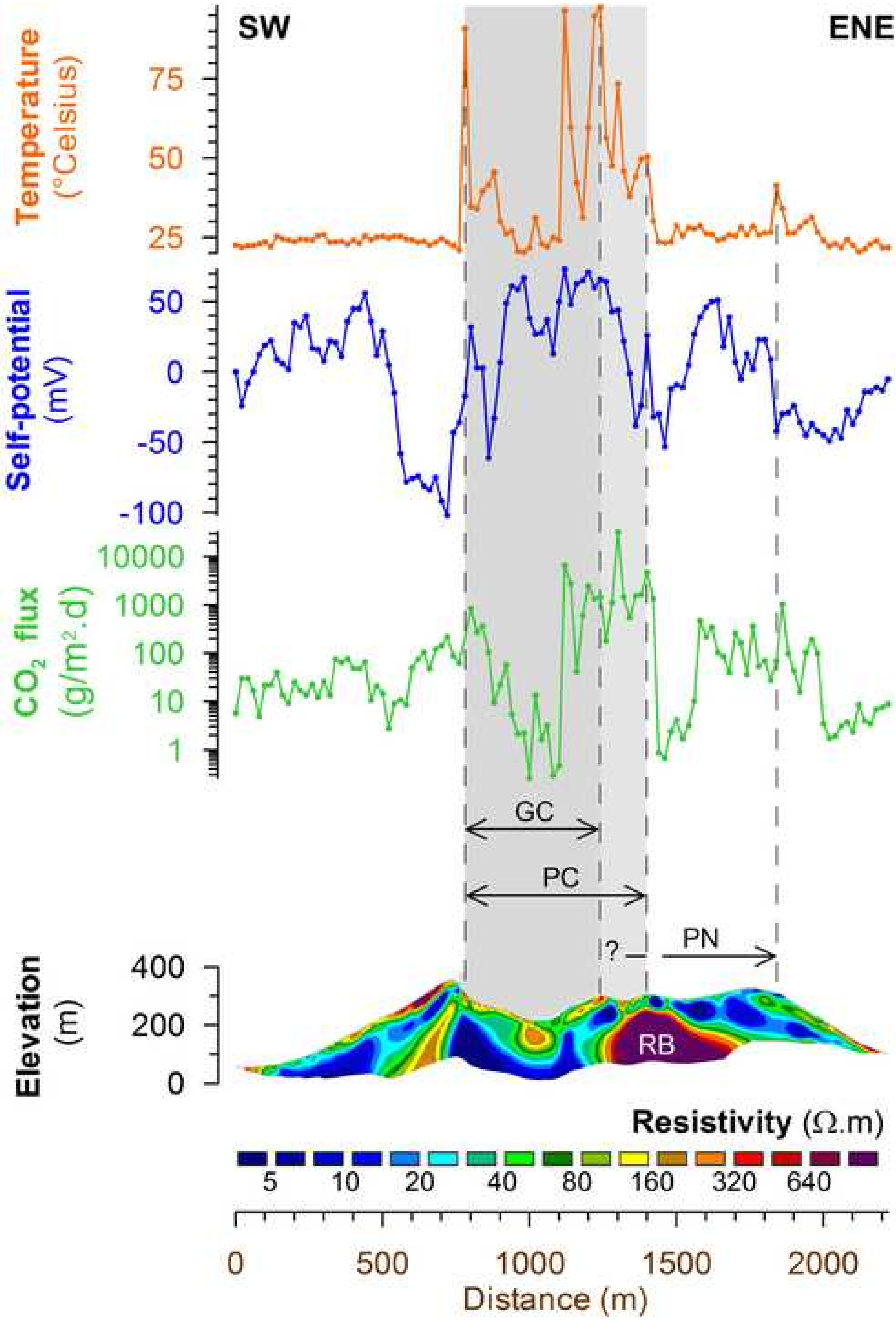

Figure 9
Click here to download high resolution image

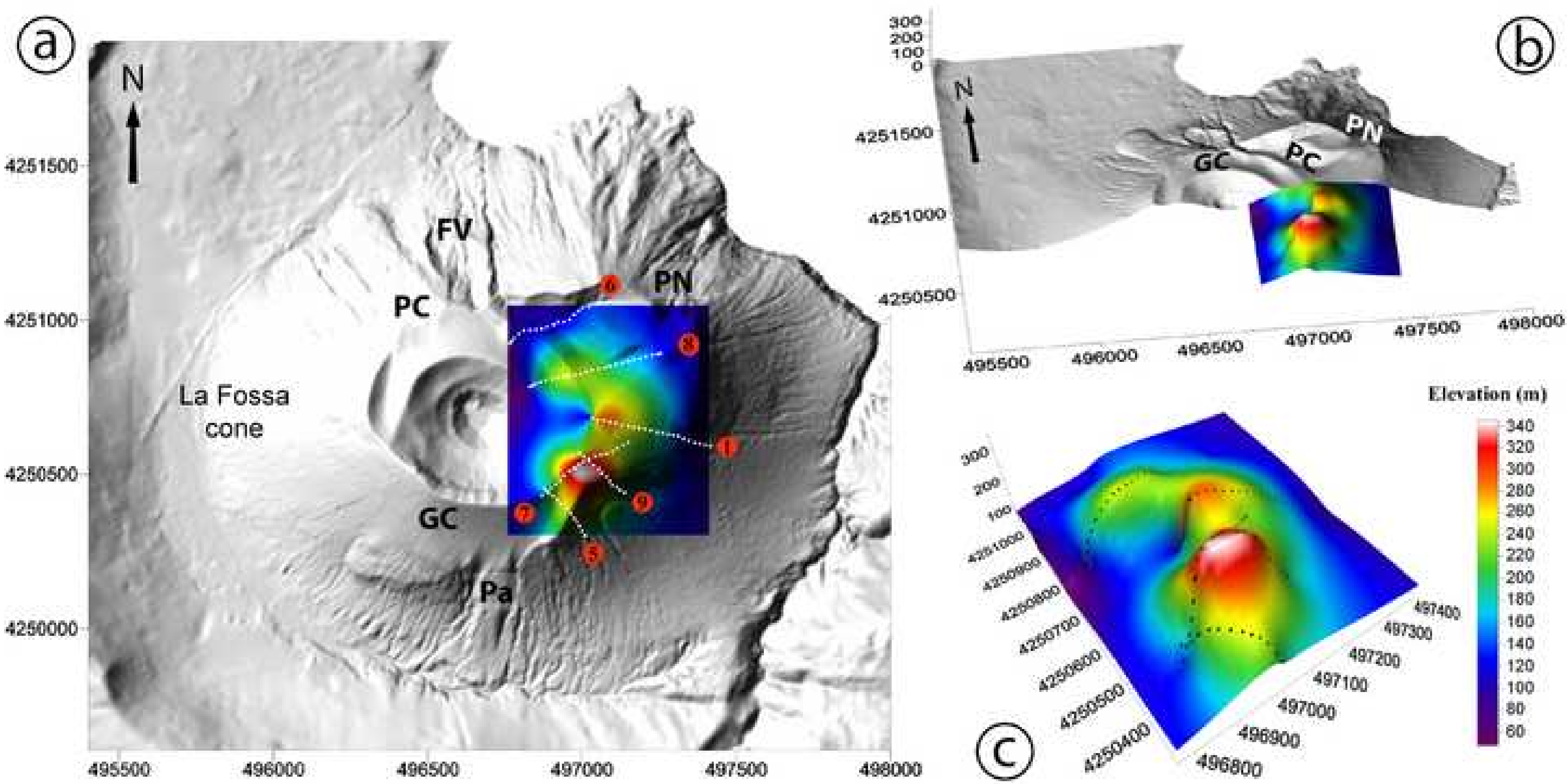

Figure 10
Click here to download high resolution image